MBoC | ARTICLE

# Loss of the HOPS complex disrupts early-to-late endosome transition, impairs endosomal recycling and induces accumulation of amphisomes

Jan van der Beek, Cecilia de Heus, Paolo Sanza, Nalan Liv, and Judith Klumperman*
Center for Molecular Medicine, University Medical Center Utrecht, Institute of Biomembranes, Utrecht University, 3584 CX Utrecht, The Netherlands

**ABSTRACT** **The multisubunit HOPS tethering complex is a well-established regulator of lysosome fusion with late endosomes and autophagosomes. However, the role of the HOPS complex in other stages of endo-lysosomal trafficking is not well understood. To address this, we made HeLa cells knocked out for the HOPS-specific subunits Vps39 or Vps41, or the HOPS-CORVET-core subunits Vps18 or Vps11. In all four knockout cells, we found that endocytosed cargos were trapped in enlarged endosomes that clustered in the perinuclear area. By correlative light-electron microscopy, these endosomes showed a complex ultrastructure and hybrid molecular composition, displaying markers for early (Rab5, PtdIns3P, EEA1) as well as late (Rab7, CD63, LAMP1) endosomes. These "HOPS bodies" were not acidified, contained enzymatically inactive cathepsins and accumulated endocytosed cargo and cation-independent mannose-6-phosphate receptor (CI-MPR). Consequently, CI-MPR was depleted from the TGN, and secretion of lysosomal enzymes to the extracellular space was enhanced. Strikingly, HOPS bodies also contained the autophagy proteins p62 and LC3, defining them as amphisomes. Together, these findings show that depletion of the lysosomal HOPS complex has a profound impact on the functional organization of the entire endosomal system and suggest the existence of a HOPS-independent mechanism for amphisome formation.**

## SIGNIFICANCE STATEMENT

- The HOPS tethering complex is a well-established regulator of lysosomal fusion. Additionally, it has proposed, but unclear roles in other pathways like endosomal maturation. By knock-out of HOPS subunits, we find an overall disorganization of the endosomal compartment..
- Specifically, we find enlarged compartments with hybrid early (Rab5, EEA1, PI3P) and late (Rab7, cathepsin D, LAMP1) endosomal markers, which we call HOPS bodies. HOPS bodies also fail to recycle CI-MPR, are not acidified (pH 5.9) and contain autophagic cargo.
- Our results suggest a broader role for HOPS in endo-lysosomal organization and a HOPS-independent mechanism by which autophagosomes fuse with endosomes.

**Monitoring Editor**
Sharon Tooze
The Francis Crick Institute

Received: Aug 29, 2023
Revised: Dec 22, 2023
Accepted: Jan 5, 2024

This article was published online ahead of print in MBoC in Press (http://www.molbiolcell.org/cgi/doi/10.1091/mbc.E23-08-0328) on January 10, 2024.

Conflicts of interest: The authors declare no financial conflicts of interests.

Author contributions: J.B., P.S., N.L., and J.K. concieved and designed the experiments; J.B., C.D., and P.S. performed the experiments; J.B. analyzed the data; J.B. and J.K. drafted the Article; J.B. prepared the digital images.

*Address correspondence to: Judith Klumperman (J.Klumperman@umcutrecht.nl).

Abbreviations used: CatD, cathepsin D; CI-MPR, cation-independent mannose-6-phosphate receptor; CLEM, correlative light-electron microscopy; CORVET, class C core vacuole/endosome tethering; EEA1, early endosomal antigen 1; EM, electron microscopy; ESCRT, endosomal sorting complexes required for transport; HOPS, homotypic fusion and vacuole protein sorting; HPF, high-pressure freezing; IF, immunofluorescence; ILVs, intraluminal vesicles; KO, knock-out; LAMP1, lysosome-associated membrane protein 1; LC3, microtubule-associated proteins 1A/1B light chain 3B; M6P, mannose-6-phosphate; PtdIns3P, phosphatidylinositol 3-phosphate; SNARE, soluble N-ethylmaleimide-sensitive factor attachment protein receptor; SNX1, sorting nexin 1; TEM, transmission electron microscope; TGN, trans-golgi network; Vps, vacuolar protein sorting; WB, western blot.

## INTRODUCTION

Membrane-bound organelles are a defining trait of eukaryotic cells. The endo-lysosomal system regulates the turnover of external and internal molecules and plays a key role in nutrient sensing and cellular homeostasis (Ballabio and Bonifacino, 2020). Disruption of the endo-lysosomal system underlies many genetic and acquired diseases, including lysosomal storage disorders, neurodegenerative diseases, and cancer (Hämälistö and Jäättelä, 2016; Lie and Nixon, 2019; Marques and Saftig, 2019).

To carry out its various tasks, the endo-lysosomal system is organized as an intricate network of distinct compartments with specialized functions. Small endocytic vesicles form by budding from the plasma membrane and fuse with early endosomes, which sort cargo for recycling back to the plasma membrane or degradation. Early endosomes mature into late endosomes (Saftig and Klumperman, 2009; Huotari and Helenius, 2011), which package membrane proteins destined for degradation into intraluminal vesicles (ILVs), or sort proteins for retrograde transport to the trans-Golgi network (TGN). Late endosomes fuse with lysosomes containing active hydrolases, after which cargo is degraded and surplus membranes retrieved for endo-lysosomal reformation (Yang and Wang, 2021). In addition, cells target intracellular cytoplasmic cargo like proteins, aggregates, and organelles for degradation by incorporation into autophagosomes (Hu and Reggiori, 2022). The forming, double membranous autophagosomes select cytoplasmic cargoes through interaction of autophagy adaptors as p62/SQSTM1 with Atg8-family proteins, such as LC3. Autophagosomes fuse with late endosomes or lysosomes, forming amphisomes or autolysosomes respectively, both eventually resulting in lysosomal degradation of the autophagic cargo (Lőrincz and Juhász, 2020). Finally, endo-lysosomal organelles play a key role in various signaling pathways (Ballabio and Bonifacino, 2020), cell-type–specific transport steps (Delevoye *et al.*, 2019) and processes such as cell division and migration (Pu *et al.*, 2016; Hämälistö *et al.*, 2020). As a whole, the endo-lysosomal system is a key regulatory system for cellular metabolism and homeostasis.

The formation of the distinct endo-lysosomal compartments requires several membrane fusion steps, which are orchestrated by specific combinations of Rab GTPases, SNAREs, and tethers. Rab GTPases are central regulators of membrane trafficking (Stenmark, 2009). After switching from a GDP-bound inactive state to a GTP-bound active state, which is promoted by Guanine Exchange Factors (GEFs), activated Rabs associate with explicit membranes and recruit various effector proteins that control protein sorting, membrane composition, organelle positioning, and fusion. Rab5 is the defining GTPase on endocytic vesicles and early endosomes, and is replaced by Rab7 on late endosomes and lysosomes (Rink *et al.*, 2005). The switch from Rab5 to Rab7 occurs during early-to-late endosomal maturation and is mediated by the Mon1–Ccz1 complex, which acts as an inhibitor of Rab5 and GEF for Rab7 (Poteryaev *et al.*, 2010; Huotari and Helenius, 2011; Langemeyer *et al.*, 2020; van den Boomen *et al.*, 2020; Herrmann *et al.*, 2023). To enact early endosome fusion events, Rab5 recruits the multisubunit tethering complex (MTC) "class C core vacuole-endosome tethering" (CORVET) (Peplowska *et al.*, 2007; Perini *et al.*, 2014; Gillingham *et al.*, 2019). Similarly, on late endosomes Rab7, possibly via or in addition to Rab2, recruits the related "homotypic fusion and vacuole protein sorting" (HOPS) complex that governs lysosomal fusion events (Rieder and Emr, 1997; Seals *et al.*, 2000; Lin *et al.*, 2014; Lőrincz *et al.*, 2017; Jongsma *et al.*, 2020; Schleinitz *et al.*, 2023;).

The HOPS complex is well characterized in yeast and mammalian cells (Seals *et al.*, 2000; Wurmser *et al.*, 2000; Balderhaar and Ungermann, 2013; Van Der Kant *et al.*, 2015;), with extensive in vitro work on its structure (Brocker *et al.*, 2012; Chou *et al.*, 2016; Shvarev *et al.*, 2022) and fusogenic activity (Zick and Wickner, 2013; Schwartz *et al.*, 2017; Song *et al.*, 2020). The HOPS complex consists of six subunits; the core units Vps11, Vps18, Vps16, and Vps33A that are shared with CORVET, and Vps39 and Vps41 that are HOPS-specific (Seals *et al.*, 2000; Van Der Kant *et al.*, 2015; van der Beek *et al.*, 2019; Shvarev *et al.*, 2022) (Figure 1A). Multiple HOPS subunits interact with Rab7 and its effectors RILP and PLEKHM1 (McEwan *et al.*, 2015; Van Der Kant *et al.*, 2015; Jongsma *et al.*, 2020; Zhang *et al.*, 2023). Additionally, Vps39 interacts with Rab2 (Kajiho *et al.*, 2016; Schleinitz *et al.*, 2023) and Vps41 with the lysosomal GTPase Arl8b (Khatter *et al.*, 2015). By acting as a tether between these GTPases, HOPS brings specific membranes in close proximity (Shvarev *et al.*, 2022). Furthermore, the core components Vps33A and Vps16 promote assembly of soluble N-ethylmaleimide-sensitive fusion protein (NSF) attachment protein receptor (SNARE) complexes (Graham *et al.*, 2013; Baker *et al.*, 2015; D'Agostino *et al.*, 2017; Song *et al.*, 2020). Complex formation of cognate SNAREs on opposing membranes drives membrane fusion. Both endo-lysosomal (VAMP7, VAMP8, Vti1b, Stx7, Stx8) (Sato *et al.*, 2000; Kim *et al.*, 2001; Collins *et al.*, 2005; Stroupe *et al.*, 2006; Collins and Wickner, 2007; Luzio *et al.*, 2009) and autophagosomal (Stx17, SNAP29) (Jiang *et al.*, 2014; Takáts *et al.*, 2014) SNAREs interact with the HOPS complex. Hence, through various interactions, the HOPS complex promotes multiple fusion events between lysosomes, late endosomes, and autophagosomes (Pols *et al.*, 2013a; Jiang *et al.*, 2014; Wartosch *et al.*, 2015).

An increasing number of studies report mutations in HOPS subunits as the cause of rare neurological disorders, often associated with dystonia (Steel *et al.*, 2020; Monfrini *et al.*, 2021a; Monfrini *et al.*, 2021b; van der Welle *et al.*, 2021; van der Beek *et al.*, 2019). On a cellular level, depletion or disruption of the HOPS complex invariably impairs endocytic progression to lysosomes and decreases autophagic flux (Pols *et al.*, 2013a; Jiang *et al.*, 2014; Wartosch *et al.*, 2015). We previously also found that small interfering RNA (siRNA)-mediated knockdown of Vps41 or Vps39 resulted in an accumulation of late endosomes (Pols *et al.*, 2013a). Additionally, depletion of HOPS components leads to phenotypes that are not straightforwardly explained by a defect in endo-lysosomal fusion. In *Drosophila*, Vps18 (*dor*) and Vps33A (*car*) mutant flies are defective in delivery of biosynthetic cathepsin D to endosomes (Sriram *et al.*, 2003) and Vps18 conditional knock-out (KO) mice accumulate the proform of cathepsin D in affected tissues (Peng *et al.*, 2012). However, Vps41 patient cells or HOPS-depleted cells still contain lysosomes with active cathepsins (Wartosch *et al.*, 2015; van der Welle *et al.*, 2021). Furthermore, the HOPS complex has been implicated in Rab GTPase switching on endosomes and lysosomes. Loss of Vps39 delays the Rab5 to Rab7 switch (Rink *et al.*, 2005) and the HOPS complex interacts with Mon1–Ccz1 (Poteryaev *et al.*, 2010). It also cooperates with SKIP, an Arl8b effector, for switch of Rab7 to Arl8b (Jongsma *et al.*, 2020). However, the precise role of the HOPS complex in Rab conversion remains elusive.

The better understand the role of the HOPS complex in vesicular trafficking pathways other than lysosomal fusion, we here investigated the effect of HOPS depletion on early–late endosome formation and function. We find that deletion of distinct HOPS subunits invariably results in the accumulation of enlarged endosomes with mixed early and late characteristics. These "HOPS bodies" are

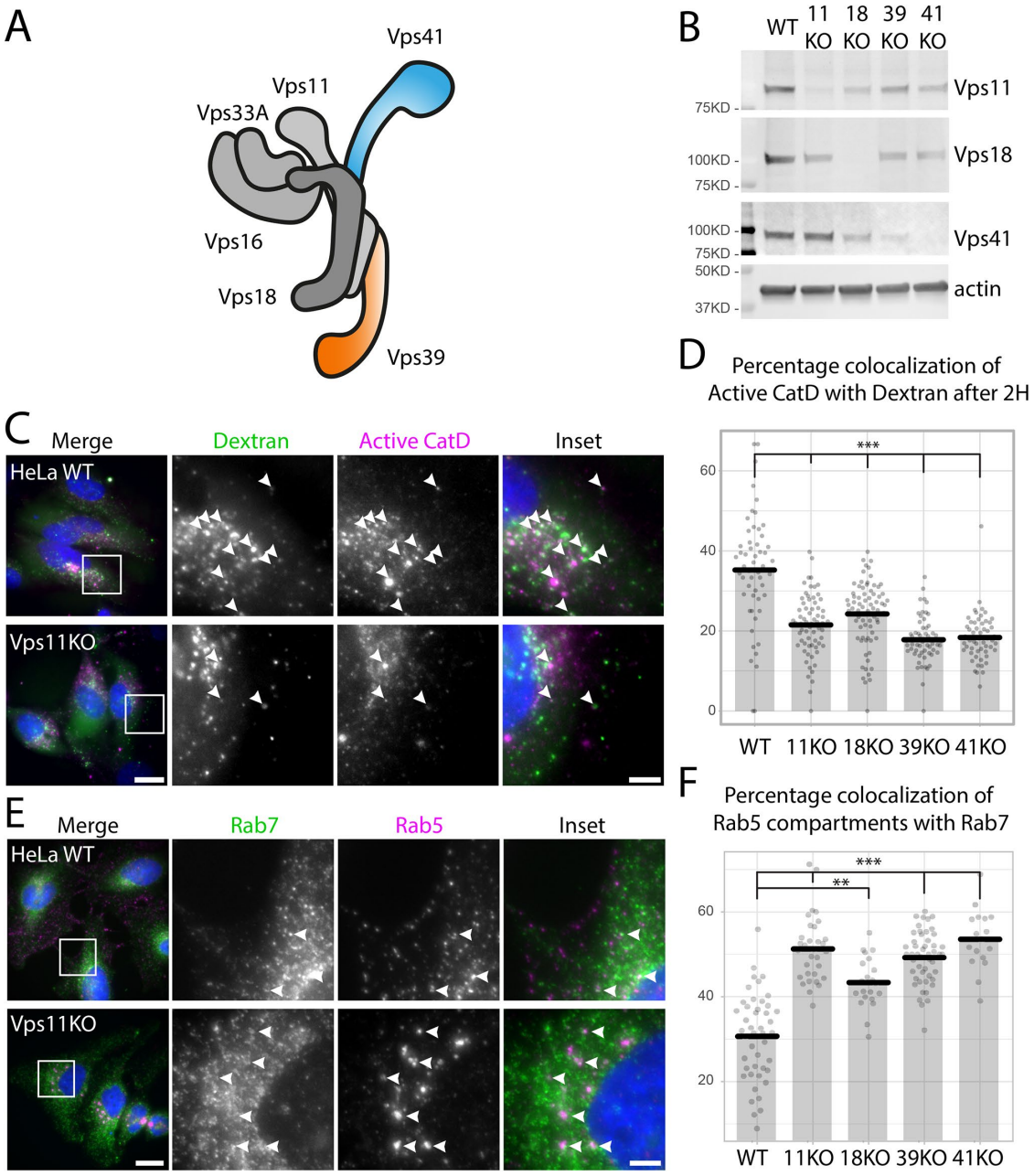


**FIGURE 1:** Depletion of HOPS increases Rab5 and Rab7 colocalization. (A) Schematic representation of the HOPS complex structure based on yeast (Shvarev *et al.*, 2022). (B) Western blot of HeLa cell lines knocked-out (KO) for HOPS subunits Vps11, Vps18, Vps39 or Vps41 by CRISPR/Cas9. KO of one subunit generally leads to a decrease in others. Vps39 KO was confirmed using DNA sequencing (van der Welle *et al.*, 2021). (C) HeLa WT and KO cells incubated with SiRlysosome, which marks active cathepsin D, and Dextran-AF488 for 2 h, fixed, and analyzed by widefield microscopy. (D) Quantification of the percentage of active cathepsin D compartments reached by endocytosed Dextran-AF488 after 2-h uptake. All HOPS Kos showed reduced colocalization, indicating that active lysosomes are poorly reached by endocytosed material, a key readout for HOPS inactivation. N ≥ 55 for each condition. (E) IF of Rab5 and Rab7 Vps11 KO cells. Enlarged Rab5 endosomes are also positive for Rab7 (arrows). (F) Quantification of Rab5-positive compartments colocalizing with Rab7 in WT cells and after KO of indicated HOPS subunits (representative images shown in Fig. S1A). Rab5 and Rab7 colocalization increases upon HOPS subunit depletion. $n = 45$, 32, 21, 49 and 17 for WT, 11KO, 18KO, 39KO, and 41KO from two independent replicates, respectively. Changes from WT are significant at $p < 0.01$ (**) or $p < 0.001$ (***), by Kruskal–Wallis multiple comparison test. Dots in dot plots represent individual cells. Scale bars 20 µm in overview images, 5 µm in insets.

enzymatically inactive, fail to recycle the cation-independent mannose-6-phosphate receptor (CI-MPR) and accumulate endocytic and autophagic cargo. Overall, our data show that loss of the HOPS complex leads to a general disruption of endosomal identity and function, highlighting a central role for HOPS in endo-lysosomal organization. Strikingly, our data also indicate that endosomes can incorporate macroautophagic material in a HOPS-independent manner.

## RESULTS

### Knockout of individual HOPS subunits invariably impairs endocytic traffic to active lysosomes

To investigate the role of the HOPS complex on the endo-lysosomal system, we generated knockout (KO) HeLa cell lines of Vps11, Vps18, Vps39, and Vps41 using CRISPR/Cas9 (van der Welle *et al.*, 2021). This selection encompassed core subunits forming the backbone of the CORVET/HOPS complex (Vps11, Vps18), as well as the HOPS-specific subunits Vps39 and Vps41 (Figure 1A). We assessed the loss of Vps11, Vps18, and Vps41 by Western blot analysis (Figure 1B) and, due to a lack of suitable antibodies, of Vps39 through genomic sequencing (van der Welle *et al.*, 2021). The Western blots confirmed deletion of Vps18 and Vps41 and showed an almost complete removal of Vps11 (>95%) in the respective KO lines. The phenotypical similarity of the Vps11 KO cell line to other HOPS KO lines in all subsequent assays indicated that the remaining band is either background, nonfunctional, or too little protein to establish fusogenic activity. The Western blot additionally revealed that upon KO of one subunit, others were also partially depleted, suggesting that subunit stability in part relies on their incorporation into the HOPS complex.

Depletion of the HOPS complex impairs delivery of endocytic cargo to active lysosomes (Pols *et al.*, 2013a; Wartosch *et al.*, 2015). Therefore, to functionally validate the different HOPS KO cell lines, we assessed in each cell line the delivery of endocytosed (2 h) Dextran conjugated to AlexaFluor (AF)-488 to enzymatically active lysosomes marked with SiRlysosome (Figure 1C) (Wartosch *et al.*, 2015; van der Welle *et al.*, 2021). Dextran-AF488 fluorescence is visible in each compartment reached by endocytosis. SiRlysosome only binds to cathepsin D in its active form, which is restricted to the acidified milieu of the lysosome. In agreement with previous studies, the percentage of SiRlysosome-positive compartments reached by Dextran-AF488 was significantly reduced in all 4 HOPS KO cells (Figure 1D). This indicated that all HOPS KO cell lines were defective in the delivery of endocytosed cargo to active lysosomes. Moreover, the data showed that the HOPS KO phenotype was not overcome by compensatory mechanisms.

### HOPS subunit depletion impairs early to late endosome maturation resulting in enlarged hybrid endosomes that cluster in the perinuclear area

Previous studies have shown that HOPS depletion delays conversion of Rab5 to Rab7, suggesting a role for HOPS in the maturation of early to late endosomes (Rink *et al.*, 2005). To assess Rab conversion in our HOPS KO cell lines, we stained for endogenous Rab5 and Rab7 by immunofluorescence (IF) and compared HeLa wild type (WT) to Vps11, Vps18, Vps39, or Vps41 KO cells. In HeLa WT cells, 25–30% of Rab5-positive endosomes was also positive for Rab7. This overlap increased to ~50% in all HOPS KO lines, in agreement with a delay in Rab5 to Rab7 conversion (Figure 1E and F; Supplementary Figure S1A). In addition, we found that hybrid Rab5-Rab7 endosomes were enlarged and clustered in the perinuclear area (Figure 1E, arrows; Supplementary Figure 2, A and B). Of note, both these phenomena were reminiscent of the phenotype seen upon expression of a constitutively active form of Rab5 (Rab5QL) (Wegener *et al.*, 2010), albeit less pronounced.

EEA1 is a tethering factor on early endosomes and effector of Rab5 (Mu *et al.*, 1995; Murray *et al.*, 2016). By double IF labeling of EEA1 and Rab5, we found that in HOPS KO cells the majority of EEA1 redistributed to the perinuclear, enlarged endosomes (Figure 2A). This redistribution was also illustrated by an overall increase in size of EEA1 compartments in HOPS KO versus WT cells (Figure 2B; Supplementary Figure S1B). We previously reported that EEA1 marks Rab5 and Phosphatidylinositol 3-phosphate (PtdIns3P)-positive endosomes, but is absent from Rab7-positive endosomes (van der Beek *et al.*, 2022). Here, in HOPS KO cells, we found that the enlarged, perinuclear Rab5 endosomes were also positive for Rab7 (Figure 1E and F; Supplementary Figure S1A). Double labeling showed that in HOPS KO cells EEA1–Rab7 colocalization was significantly increased (18–32% in KO cells) compared with WT cells (10%; Supplementary Figure S1, C and D), with both proteins strongly enriched on the enlarged, perinuclear endosomes. Because EEA1 IF distinctively highlighted the population of hybrid Rab5-Rab7–positive endosomes, we used EEA1 as marker for these organelles in our subsequent microscopy studies.

PtdIns3P is an interactor of EEA1 and important for endosomal maturation (Huotari and Helenius, 2011). Recently, we showed by correlative light-electron microscopy (CLEM) the existence of a subpopulation of EEA1 and PtdIns3P-positive endosomes that by morphology was classified as late endosomal (van der Beek *et al.*, 2022). To investigate whether the enlarged, perinuclear Rab5-Rab7-EEA1 endosomes in HOPS KO cells also contained PtdIns3P, we transfected these with a 2xFYVE-mCherry construct, a genetic reporter that specifically binds PtdIns3P (Gillooly *et al.*, 2003) (Figure 2C). By fluorescence microscopy, we indeed found PtdIns3P on the typical, EEA1-positive enlarged endosomes in HOPS KO cells. To establish whether these Rab5-Rab7-EEA1-PtdIns3P endosomes still formed recycling tubules, we performed IF of Vps35, a component of the Retromer complex. Retromer controls the recycling of a variety of cargos to either the TGN or plasma membrane (Burd and Cullen, 2014). Both in WT and Vps11 KO cells, we readily found Vps35-positive structures associated with EEA1-positive endosomes (Supplementary Figure S2A), suggesting that the hybrid endosomes were still capable of forming recycling tubules. To further assess the recycling capacity in HOPS KO cells, we performed a pulse chase experiment with Transferrin-AlexaFluor488 (Tf-488), a general marker for endosome to plasma membrane recycling (Supplementary Figure S2, B and C). After 5-min uptake, in both WT and HOPS KO cells Tf-488 was found in EEA1-positive compartments (at 30–50% colocalization). We then chased with normal medium for 10 or 30 min, which is known to deplete cells from Tf-488 by recycling and release into the medium. Correspondingly, a 10-min chase in HeLa WT cells decreased the colocalization of Tf-488 with EEA1 to only 7% and after 30 min Tf-488 was barely detectable (colocalization with EEA1 <1%). Strikingly, the HOPS KO cells showed a very similar pattern, with after 10-min chase only 3–12% colocalization and less than 1% colocalization after 30-min chase. These results indicated that recycling from endosomes to the plasma membrane remained unaffected in HOPS KO cells.

Together, these results showed that HOPS KO induced the accumulation of enlarged EEA1-Rab5-PtdIns3P-Rab7-Vps35–positive endosomes in the perinuclear area. The hybrid early–late molecular composition of these endosomes suggested a block or delay in the Rab5-Rab7 switch. The data also showed that HOPS was not required to establish PtdIns3P levels on endosomes or to recycle Tf to the plasma membrane.

### HOPS KO–induced hybrid endosomes contain inactive lysosomal enzymes

Whereas the role of HOPS complex in lysosomal fusion is well established, studies on the role of HOPS in the delivery of lysosomal enzymes are conflicting (Sriram *et al.*, 2003; Swetha *et al.*, 2011; Peng *et al.*, 2012). To investigate a putative effect of HOPS KO on lysosomal enzyme transport, we used a pan-cathepsin D antibody

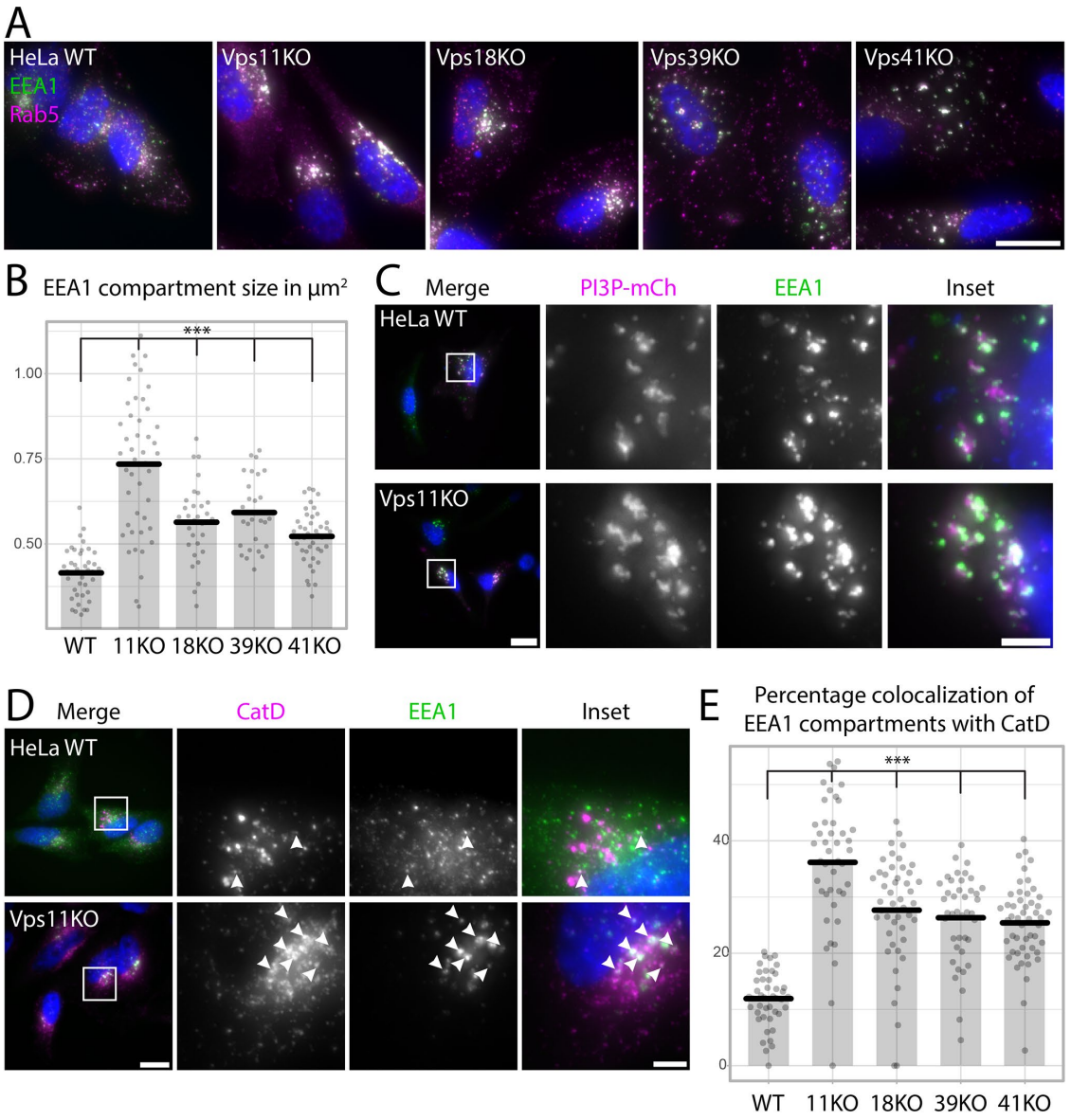


**FIGURE 2:** HOPS KO cells accumulate enlarged endosomal compartments with mixed early and late endosomal proteins. (A) Enlarged, perinuclear Rab5-positive compartments in HOPS KO cells specifically accumulate EEA1 label. (B) Quantification of EEA1 compartment size. Based on thresholded pixel counts in confocal images (shown in Supplementary Figure S1B), $n \geq 27$ from two independent replicates for each condition. (C) IF staining for EEA1 in cells transfected with the 2xFYVE-mCherry probe for PtdIns3P. Strong colocalization is observed in both HeLa WT and Vps11 KO cells. (D) IF staining for cathepsin D and EEA1 reveals striking colocalization in Vps11 KO cells, whereas colocalization in HeLa WT cells is minimal. (E) Quantification of the percentage of EEA1-positive compartments colocalized with cathepsin D, including other KOs (IF examples shown in Fig. S3A). $n \geq 41$ from two independent replicates for each condition. Changes from WT are significant at $p < 0.001$ (***), by Kruskal–Wallis multiple comparison test. Dots in dot plots represent cell averages (B) or individual cell values (E). Scale bars 20 µm in overview images, 5 µm in insets.

to label both active and inactive forms of the enzyme. In HeLa WT cells, the percentage of EEA1 compartments that contained cathepsin D was only ~12%, reflecting its predominantly late endo-lysosomal steady-state distribution. In contrast, in HOPS KO cells cathepsin D was found in 25–40% of the EEA1-positive hybrid compartments (Figure 2D and E; Supplementary Figure S3A), indicating that HOPS KO caused the accumulation of lysosomal enzymes in these enlarged endosomes. Moreover, labeling for CD63 and LAMP1 also showed a significant overlap with EEA1, indicating that the enlarged endosomes also contained late endosomal–lysosomal membrane proteins (Supplementary Figure S3, B–E). Because wide-field microscopy has a limited resolution especially in the z-axis, we then performed fluorescence labeling of 150 nm–thick thawed cryosections. With the improved z-resolution, we found striking examples of colocalization for EEA1, LAMP1, and cathepsin D in HOPS KO cells (Supplementary Figure S3, F and G). Together, these data unequivocally showed that the enlarged endosomes induced by HOPS KO contained a mixed set of early endosomal proteins, late endo-lysosomal regulators, lysosomal enzymes, and membrane proteins.

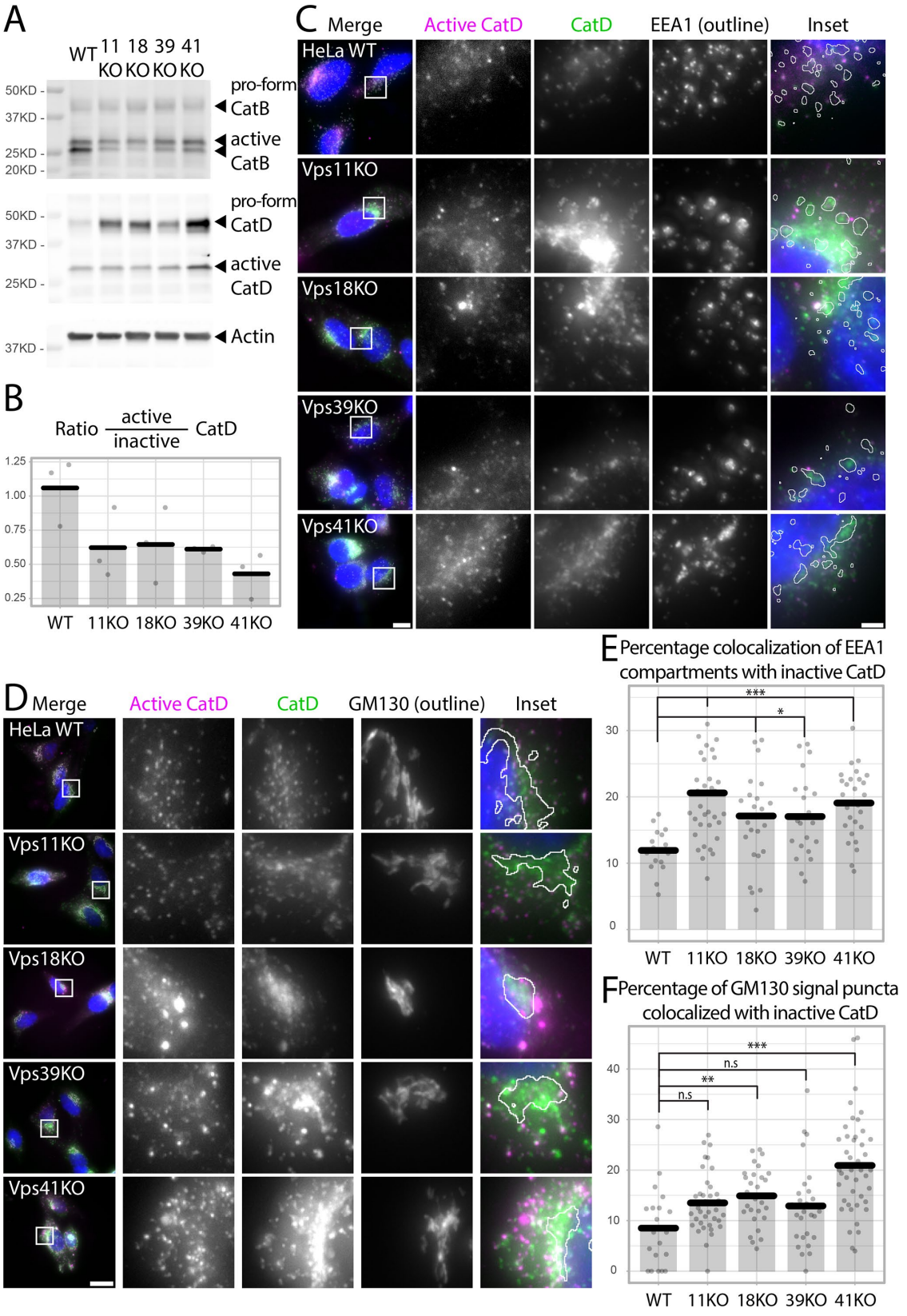


FIGURE 3: HOPS KO impairs cathepsin B and D processing to their active forms. (A) Western blot of cathepsin B and cathepsin D showing relative enrichment of pro-forms in HOPS KO cells. (B) Quantification of the ratio active over inactive cathepsin D as shown in A. Based on three independent replicates, dots represent individual replicate values. (C) Combined staining for pan-cathepsin D and active cathepsin D using antibody and SiRlysosome, respectively. Additional IF of EEA1 showed colocalization with pan-cathepsin D but not SiRlysosome signal. Inset is enlargement of outlined area. (D) IF staining as in B, but with Golgi marker GM130 instead of EEA1. Pan-cathepsin D staining is

To extend these observations to other cell types, we next generated A549 cell lines KO for Vps18 and Vps41, and HT1080 cells KO for Vps18 and Vps39. We validated these lines using Western blot (Supplementary Figure S4, A and B) or, in the case of the HT1080 Vps39 KO, genomic sequencing (Supplementary Figure S4C; and Materials and Methods). As a key defining experiment for the HOPS KO phenotype found in HeLa cells, we performed Rab7-EEA1 and cathepsin D-EEA1 colocalization by IF. Although the base level of colocalization differed between the respective WT lines, HOPS depletion invariably increased the level of colocalization between these early and late endosomal markers (Supplementary Figure S4, D–I). These data showed the formation of hybrid early–late endosomes by HOPS KO was a consistent phenotype, found in multiple cell types.

Activation of cathepsins requires processing into their mature forms, which generally involves an acidified environment and cleavage by other proteases (Laurent-Matha *et al.*, 2006; Yadati *et al.*, 2020). To investigate the activity of lysosomal hydrolases in HOPS KO cells, we analyzed the ratio of the active mature forms over the inactive proforms by Western blot. This showed a striking decrease for cathepsin D in HOPS KO compared with HeLa WT cells, indicating a relative enrichment in the profrom (Figure 3A and B). A less striking but similar effect was seen for cathepsin B (Figure 3A). Next, to determine the subcellular localization of inactive versus active cathepsin D, we combined the pan-cathepsin D antibody with the SiRlysosome probe in fluorescent microscopy. In this setup, organelles labeled for pan-cathepsin D but not SiRlysosome will only contain inactive cathepsin D. In HeLa WT cells, pan-cathepsin D and SiRlysosome signals largely overlapped and showed little colocalization with EEA1, indicating that the vast majority of cathepsin D was active and localized in late endo-lysosomal compartments (Figure 3C). Strikingly, in HOPS KO cells the pan-cathepsin D label colocalized less with SiRlysosome (Figure 3C; Supplementary Figure S5A) and significantly colocalized with the enlarged, EEA1-positive endosomes where the SiRlysosome signal was generally absent (Figure 3C and E). Thus, the cathepsin D present in the hybrid endosomes induced in HOPS KO cells was predominantly inactive. Further examination of the pan-cathepsin D labeling in HOPS KO cells revealed an additional pool of cathepsin D in the perinuclear area that was not labeled for EEA1 (Figure 3C). Combining pan-cathepsin D and SiRlysosome staining with the Golgi or TGN markers GM130 or TGN46 (Figure 3D and F; Supplementary Figure S5B), showed a clear increase in this Golgi/TGN pool of inactive cathepsin D in the HOPS KO cells. Together, these experiments showed that HOPS KO cells accumulated inactive cathepsin D in the Golgi/TGN area as well as in the hybrid early–late endosomes marked by EEA1.

The altered distribution and activity of cathepsin D in HOPS KO cells indicated a defect in lysosomal enzyme trafficking. In case lysosomal enzymes lack a mannose-6-phosphate tag, they are in the TGN incorporated in the default secretory pathway and released into the culture medium (Reitman *et al.*, 1981). To assess if this was also the case in HOPS KO cells, we concentrated proteins of serum-free culture medium from HeLa WT and HOPS KO cells by TCA precipitation. The resulting culture medium concentrates were analyzed by Western blot. This revealed an increase in secreted proforms of cathepsins B, D, and L in all HOPS KO cells (Supplementary Figure S5C).

Combined, our data demonstrated that HOPS KO resulted in the peri-nuclear accumulation of enlarged endosomal compartments that acquired late endo-lysosomal proteins (LAMP1, inactive cathepsin D, CD63, Rab7; Figure 2D; Supplementary Figures S1C and S3, B and D), while early endosomal markers (Rab5, EEA1, PtdIns3P, Vps35; Figure 2A and C; Supplementary Figures S1C and S2A) were still present. The data imply that HOPS KO led to an impairment in early to late endosomal maturation and decreased activation of lysosomal enzymes. For clarity, we will further refer to the hybrid endosomal compartments as "HOPS bodies."

### HOPS depletion impairs retrograde recycling of CI-MPR

Most lysosomal enzymes, including cathepsin D, depend on the CI-MPR for trafficking to lysosomes. Lysosomal enzymes are tagged with a mannose-6-phosphate (M6P) group in the Golgi complex that is recognized by the CI-MPR in the TGN (Hille-Rehfeld, 1995; Braulke and Bonifacino, 2009). CI-MPR and its bound ligands exit the TGN in clathrin-coated vesicles that traffic to early endosomes (Klumperman *et al.*, 1993; Waguri *et al.*, 2003). After substrate release in the acidified milieu of late endosomes, CI-MPR travels back to the TGN by a retrograde pathway dependent on ESCPE, a complex formed by SNX1/2 and 5/6 (Mari *et al.*, 2008; Evans *et al.*, 2020; Simonetti *et al.*, 2023). Our findings that HOPS KO led to the accumulation of inactive cathepsin D in the Golgi/TGN (Figure 3D and F; and Supplementary Figure S3) raised the question whether CI-MPR trafficking was disrupted in these cells.

To address this, we performed IF staining of CI-MPR in combination with TGN46, SNX1, and/or EEA1 in HeLa WT and HOPS KO cells. In HeLa WT cells, the majority of CI-MPR was present in the TGN (Figure 4A, white outlines), which is in agreement with many previous studies (Brown and Farquhar, 1984; Brown *et al.*, 1984; Seaman, 2004; Styers *et al.*, 2004). The CI-MPR signal outside the TGN partially colocalized with EEA1 (WT in Figure 4C and D) and more strikingly with SNX1 (WT in Figure 4A and B), indicative for the retrograde pathway from endosomes to TGN. Strikingly, in HOPS KO cells, the majority of CI-MPR signal localized to the EEA1-positive HOPS bodies (Figure 4C and D), outside the Golgi area (Figure 4A and B). Since by Western blot the overall levels of CI-MPR were not higher in the HOPS KO cells (Figure 4E), this altered staining pattern indicated a redistribution of CI-MPR rather than increased levels in endosomes due to decreased degradation. In addition, the overall colocalization of CI-MPR with SNX1 had decreased in all HOPS KO cells (Figure 4A and B), suggesting a blockade in retrograde transport.

To reveal the association of CI-MPR with SNX1 in ultrastructural detail, we performed immuno-electron microscopy (immuno-EM) of WT and HOPS KO cells using immunogold labeling of cryosections (Figure 5A–D; Supplementary Figure S6). HOPS KO cells contained a characteristic population of enlarged endosomes with mixed early and late morphological features which we identified as HOPS bodies (see below and Figures 7 and 8). Quantitation of the relative

enriched in the Golgi area, which lacks SiRlysosome. (E) Quantification of C based on spot detection. Percentage of EEA1-positive compartments colocalized with pan-cathepsin D without SiRlysosome signal, n ≥ 17 for each condition. (F) Quantification as in E. The percentage of GM130 compartments positive for pan-cathepsin D but not SiRlysosome increased in HOPS KO cells. n ≥ 22 per condition. Changes from WT are significant at $p < 0.05$ (*), $p < 0.01$ (**) or $p < 0.001$ (***) or not significant (n.s.), by Kruskal–Wallis multiple comparison test. Dots in the dot plots represent individual cells. Scale bars 20 μm in overview images, 5 μm in insets.

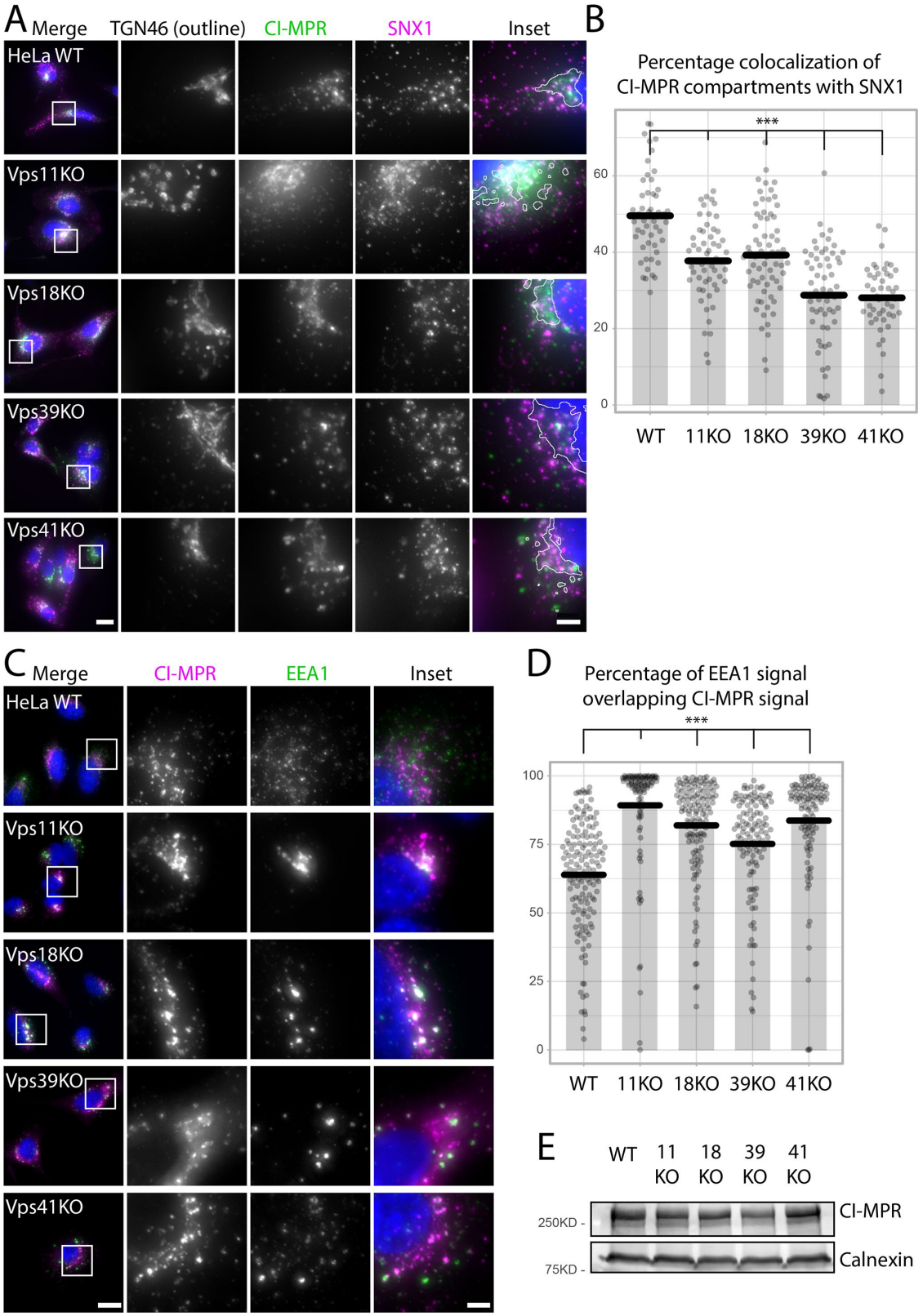


FIGURE 4: HOPS depletion impairs CI-MPR retrograde transport. (A) IF of SNX1, CI-MPR and TGN46 reveals reduced colocalization of SNX1 and CI-MPR. Outlines in insets represent TGN46 signal. (B) Quantification of CI-MPR colocalization with SNX1. n ≥ 48 from 2 independent replicates for each condition. (C) IF of CI-MPR and EEA1 in HeLa WT and HOPS KO cells. CI-MPR redistributes to EEA1-positive compartments in HOPS KO cells. (D) Quantification of C as the percentage of thresholded EEA1 signal overlapping thresholded CI-MPR signal. n ≥ 43 per condition from two independent replicates. (E) Western blot of CI-MPR shows no significant increase in HOPS KO cells. Changes from WT are significant at $p < 0.05$ (*), $p < 0.01$ (**) or $p < 0.001$ (***) by Kruskal–Wallis multiple comparison test. Dots in dot plots represent individual cells. Scale bars 20 μm in overviews, 5 μm in insets.

distribution of CI-MPR (Figure 5E) showed that the fraction of CI-MPR in endosomes strikingly increased in Vps18 KO (59%) compared with WT (17%) cells, whereas the percentage in the TGN was strikingly decreased (39% in WT to 18% in Vps18 KO, Figure 5E). Double labeling of CI-MPR with SNX1 showed that in HeLa WT cells 58% of the SNX1 endosomal tubules were also positive for CI-MPR (Figure 5A and C, arrowheads, F). In HOPS KO cells, SNX1-positive vesicles and tubules were still readily found near endosomes/HOPS bodies (Figure 5D; Supplementary Figure S6, blue pseudocolor), but the percentage that also contained CI-MPR had decreased to 38% (Figure 5D and F; Supplementary Figure S6).

The findings in Figures 4 and 5 and Supplementary Figure S6 altogether demonstrated that CI-MPR was depleted from the TGN and redistributed to endosomes upon HOPS KO. We still found SNX1-positive recycling tubules on endosomes in HOPS KO cells, but CI-MPR failed to efficiently enter these. Impairment of retrograde transport to the TGN explained the relative shift in CI-MPR localization from TGN toward endosomes.

### HOPS bodies are not acidified

What could prevent the CI-MPR from entering SNX1 recycling tubules? Retrograde transport of CI-MPR presumably depends on ligand dissociation, which allows CI-MPR to engage in further rounds of hydrolase sorting at the TGN (Brown *et al.*, 1984; Brown *et al.*, 1986; Braulke and Bonifacino, 2009). Dissociation between acid hydrolases and CI-MPR is induced by acidification of maturing endosomes (Brown *et al.*, 1986; Olson *et al.*, 2020). To test if the impairment of CI-MPR recycling could be caused by an acidification defect of HOPS bodies, we treated HeLa WT and Vps18 KO cells for 3 h with Chloroquine or Bafilomycin A1. Chloroquine is a weak base that accumulates and neutralizes acidified compartments (Homewood *et al.*, 1972), while Bafilomycin A1 blocks the V-ATPase, preventing endo-lysosomal acidification (Bowman *et al.*, 1988; Yoshimori *et al.*, 1991). In HeLa WT cells, both drugs caused a statistically significant redistribution of CI-MPR to EEA1-positive endosomes (Figure 6A-B), which is in agreement with previous studies (Brown *et al.*, 1984; Brown *et al.*, 1986; van Weert *et al.*, 1995). In contrast, in Vps18 KO cells we found no additional effect of the drugs on CI-MPR redistribution. These data implied that impaired retrograde recycling of CI-MPR in HOPS KO cells could be due to a lack of acidification of HOPS bodies.

To assess the pH of HOPS bodies, we performed live-cell imaging of cells incubated for 3 h with Dextran-fluorescein. Fluorescein fluorescence is pH-sensitive under excitation with 480 nm but not 440 nm light, making it a robust ratiometric pH sensor (Canton and Grinstein, 2015). To address HOPS bodies specifically, and not all endocytic compartments, we imaged HeLa WT, Vps18, and Vps39 KO cells stably expressing EEA1-mCherry. We first calibrated our fluorescence readout by imaging pH-clamped HeLa WT cells (see *Materials and Methods*; Supplementary Figure S7) and then imaged the EEA1-mCherry–expressing lines in normal culture medium. We found that the ratio of fluorescein 440/480 intensity in the EEA1-positive compartments corresponded to an average pH of 5.7 in WT cells and 5.9 in both Vps18 and Vps39 KO cells (Figure 6C and D). This demonstrated that the HOPS bodies, though they acquire late endosomal characteristics, undergo only mild acidification typical for early stages of the endo-lysosomal system (Huotari and Helenius, 2011).

Overall, these data indicated that a key aspect of late endosomal maturation – that is, acidification – is impaired in HOPS bodies. Because a lack of acidification prevents CI-MPR–ligand dissociation, the near neutral pH in HOPS bodies is a likely explanation for the observed accumulation of CI-MPR.

### HOPS bodies have a mixed early and late morphology and receive endocytic cargo

EM is the method of choice to link molecular composition to cellular ultrastructure and has been exceptionally insightful in characterization of the endo-lysosomal system (Klumperman and Raposo, 2014). The immuno-EM of CI-MPR and SNX1 (Figure 5; Supplementary Figure S6) already revealed endo-lysosomal organelles of peculiar morphology, presumably representing the HOPS bodies. Unfortunately, our marker to label HOPS bodies by IF, EEA1, labels poorly in immuno-EM (van der Beek *et al.*, 2022), hampering correlation between our IF and EM data. To overcome this, we used our recently developed on-section CLEM method to localize proteins in EM based on their IF staining (van der Beek *et al.*, 2022).

HeLa WT and Vps18 KO cells were incubated with the endocytic tracer bovine serum albumin conjugated to 5-nm gold particles ($BSA^5$) for 3 h, fixed with 4% formaldehyde, and prepared for cryosectioning. Ultrathin cryosections were fluorescently labeled and scanned by fluorescence microscopy for EEA1-positive compartments. Then the same sections were transferred to EM and correlated to the IF signal. In EM, distinct types of endo-lysosomal compartments were defined by their morphology (see *Materials and Methods* for detailed definitions). Consistent with our previous findings (van der Beek *et al.*, 2022), in HeLa WT cells EEA1 was present on early endosomes (electron lucent vacuoles partially coated with clathrin and displaying associated tubules) (Figure 7A), as well as late endosomes (rounded to oval shaped organelles with ≥6 ILVs) (Figure 7A). Lysosomes (small-sized compartments with amorphous electron-dense content and sometimes "onion-like" concentric membranes) generally lacked EEA1. In HOPS KO cells, EEA1 also localized to "classical" early and late endosomes, but additionally associated with numerous enlarged compartments of complex ultrastructure, the HOPS bodies (Figure 7B and D–F; Supplementary Figure S8, A–E). Quantitation of the relative distribution of EEA1 in HeLa WT versus Vps18 KO cells showed a significant redistribution of EEA1 label to the HOPS bodies (Figure 7C), in line with the IF data (Figure 2). The EEA1-positive HOPS bodies were identical to the compartments in which we found accumulation of CI-MPR (Figure 5; Supplementary Figure S6)

EM analysis of the HOPS bodies disclosed them as large vacuoles that regularly displayed clathrin coats at the cytosolic face of their limiting membrane and associated tubules that extended from the vacuolar part. The clathrin coat is indicative for the presence of ESCRT and ongoing ILV formation, whereas the tubules mediate recycling, which are both features of early endosomes (Raiborg *et al.*, 2002; Klumperman and Raposo, 2014). In addition, the lumen of the HOPS bodies exhibited numerous ILVs, membrane whorls, and electron-dense material, which are characteristic of late endosomes-lysosomes. Furthermore, HOPS bodies regularly contained endocytosed $BSA^5$ and amorphous, granular material indicative of lipid accumulation. This is consistent with previous findings from (Anderson *et al.*, 2022), who found an endo-lysosomal accumulation of cholesterol upon KO of Vps41 and Vps39.

We next fixed HeLa WT and various HOPS KO cells by high-pressure freezing (HPF) for resin EM. HPF fixation is less appropriate for immuno-EM, but the prime approach for purely ultrastructural studies. Moreover, the high contrast and large size of resin EM sections makes them optimal for systematic morphological analyses. After HPF fixation, HOPS bodies were readily recognized as enlarged vacuoles containing a mix of membranes, amorphous content and ILVs and displaying clathrin coats and associated tubules (Figure 8D–G). Strikingly, in low magnification overviews we found in all HOPS KO cells an accumulation of HOPS bodies as well as an overall

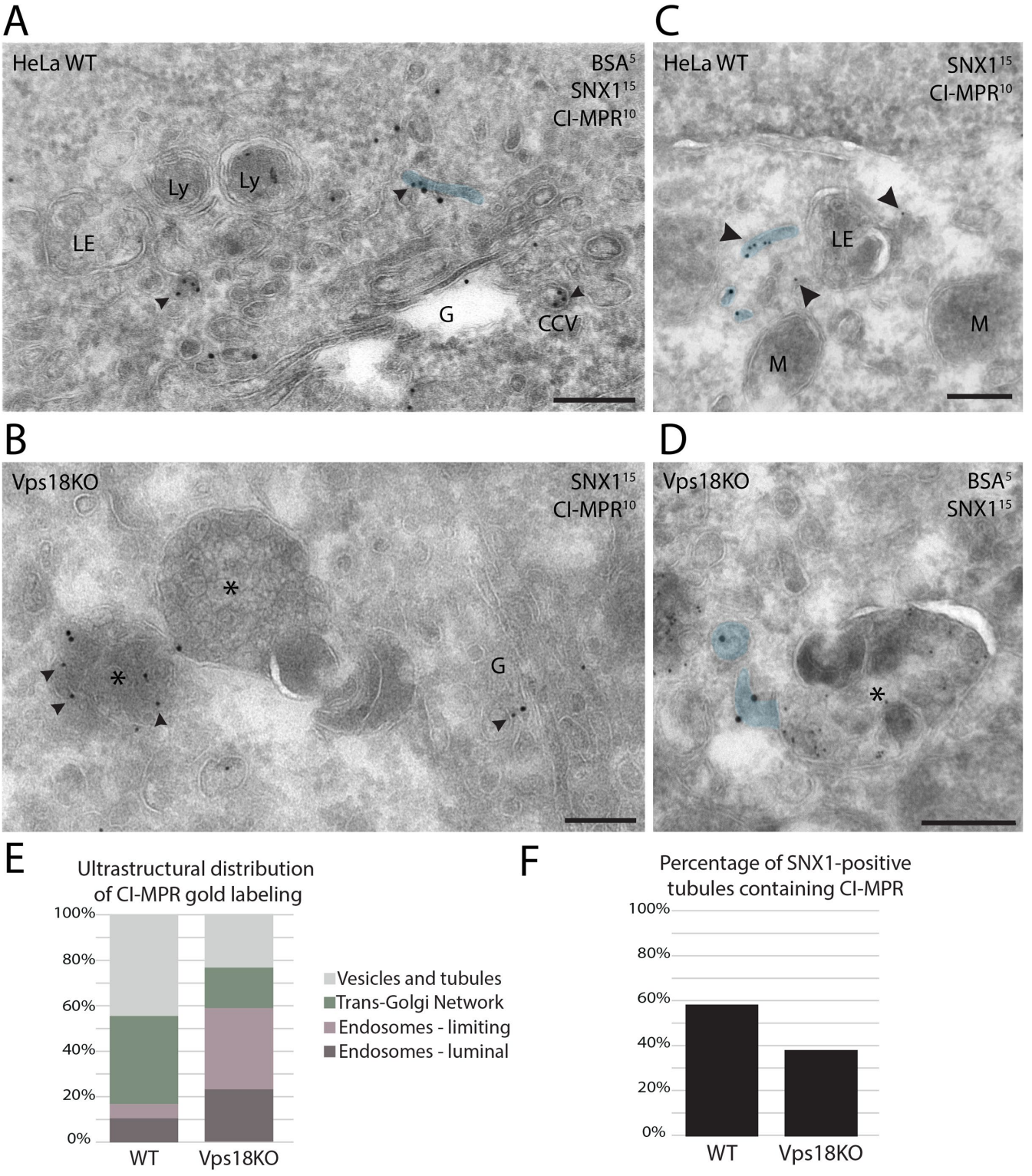


**FIGURE 5:** CI-MPR does not enter SNX1-positive tubules in HOPS KO cells. Immuno-EM of SNX1 (15 nm gold) and CI-MPR (10 nm gold) in HeLa WT (A, C) and Vps18 KO (B, D) cells. In (A) and (D), endocytic tracer BSA$^5$ was added to cells 3 h before fixation. SNX1-positive tubules are highlighted in blue. In WT cells SNX1-positive tubules contain CI-MPR (arrows). In Vps18 KO cells CI-MPR accumulates in the lumen of the HOPS bodies (B, asterisks), despite the presence of associated SNX1-positive tubules (D, highlighted blue). See Supplementary Figure S6 for additional pictures and other HOPS KO cells. (E) Quantification of CI-MPR immunogold labeling. CI-MPR is depleted from TGN in Vps18 KO cells. Within endosomes, CI-MPR is enriched in both the limiting membrane and lumen. n > 300 gold particles per condition. (F) Quantification of the percentage of SNX1-positive tubules also positive for CI-MPR labeling, $n = 58$ and 105 SNX1-positive tubules for WT and Vps18 KO, respectively. *, HOPS body; G, Golgi; M, mitochondrion; LE, late endosome; Ly, lysosome. Scale bars 200 nm.

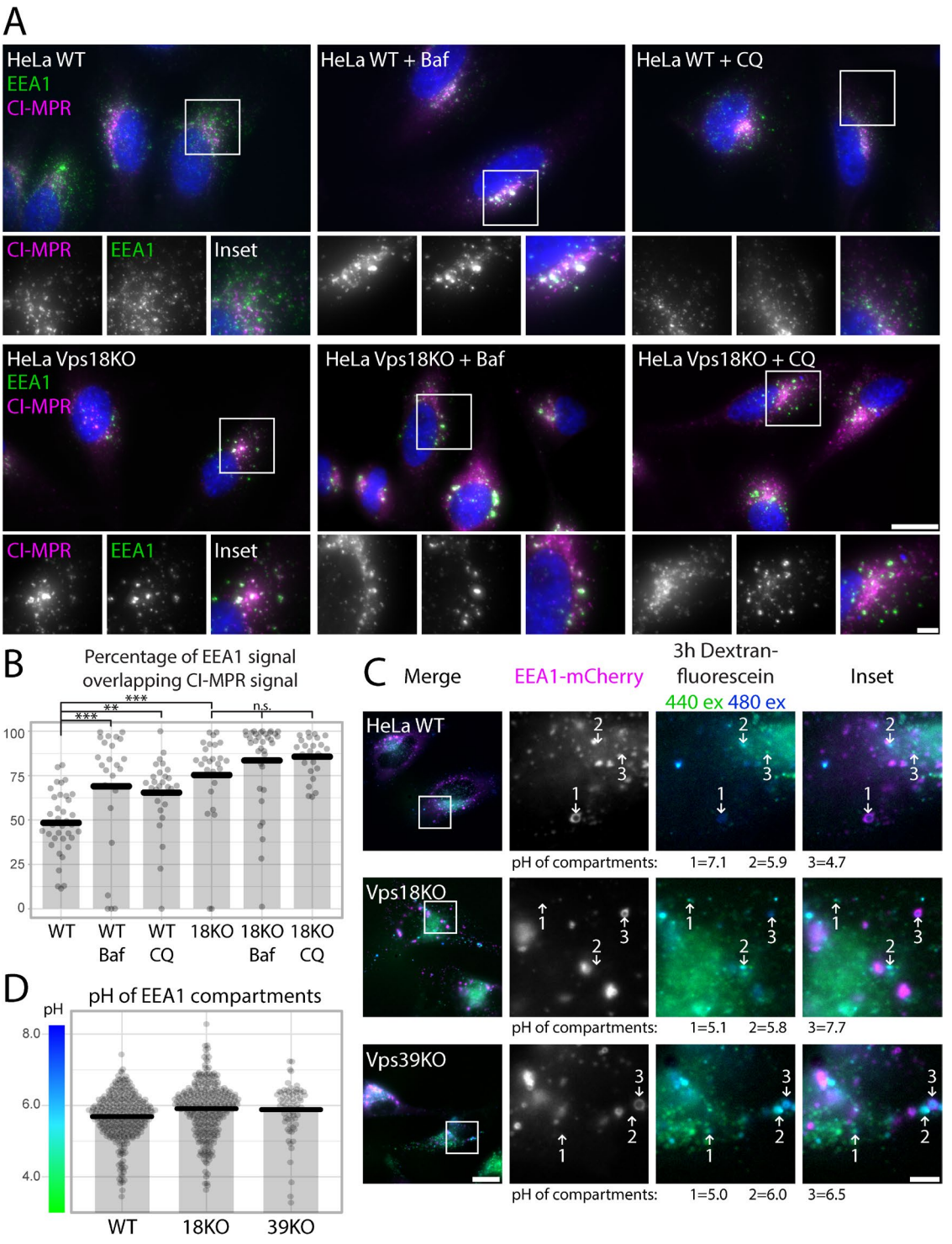


**FIGURE 6:** Elevated pH inhibits retrograde CI-MPR transport from HOPS bodies. (A) IF of CI-MPR and EEA1 in HeLa WT and Vps18 KO cells, untreated or treated with Bafilomycin A1 (Baf) or Chloroquine (CQ) for 3 h. (B) Quantification of the percentage of thresholded EEA1 signal overlapping with CI-MPR signal. n ≥ 24 for each condition. In Baf- or CQ-treated HeLa WT cells CI-MPR disperses to EEA1-positive compartments to the same level as in nontreated Vps18 KO cells. In Vps18 KO cells treatment has no additional effect. (C) Live-cell fluorescence imaging of WT, Vps18 and Vps39 KO cells expressing EEA1-mCherry, incubated for 3 h with Dextran-fluorescein. The ratio of 440/480 excitation of fluorescein serves as a pH sensor. This ratio is translated to actual pH using calibration samples described in Supplementary Figure S7. Several examples of individual pH measurements on compartments are shown. (D) Quantification of the 440/480 ratios found in EEA1 compartments of HeLa WT, Vps18, and Vps39 KO cells. $n = 324$, 310, and 68 EEA1 compartments from ≥ 10 cells from WT, Vps18, and Vps39 KO, respectively. Changes between conditions are significant at $p < 0.01$ (**) or $p < 0.001$ (***) or not significant (n.s.), by Kruskal–Wallis multiple comparison test. Dots in dot plots represent individual cells (B) or single EEA1 compartments (D). Scale bars 20 μm (overviews), 5 μm (insets).

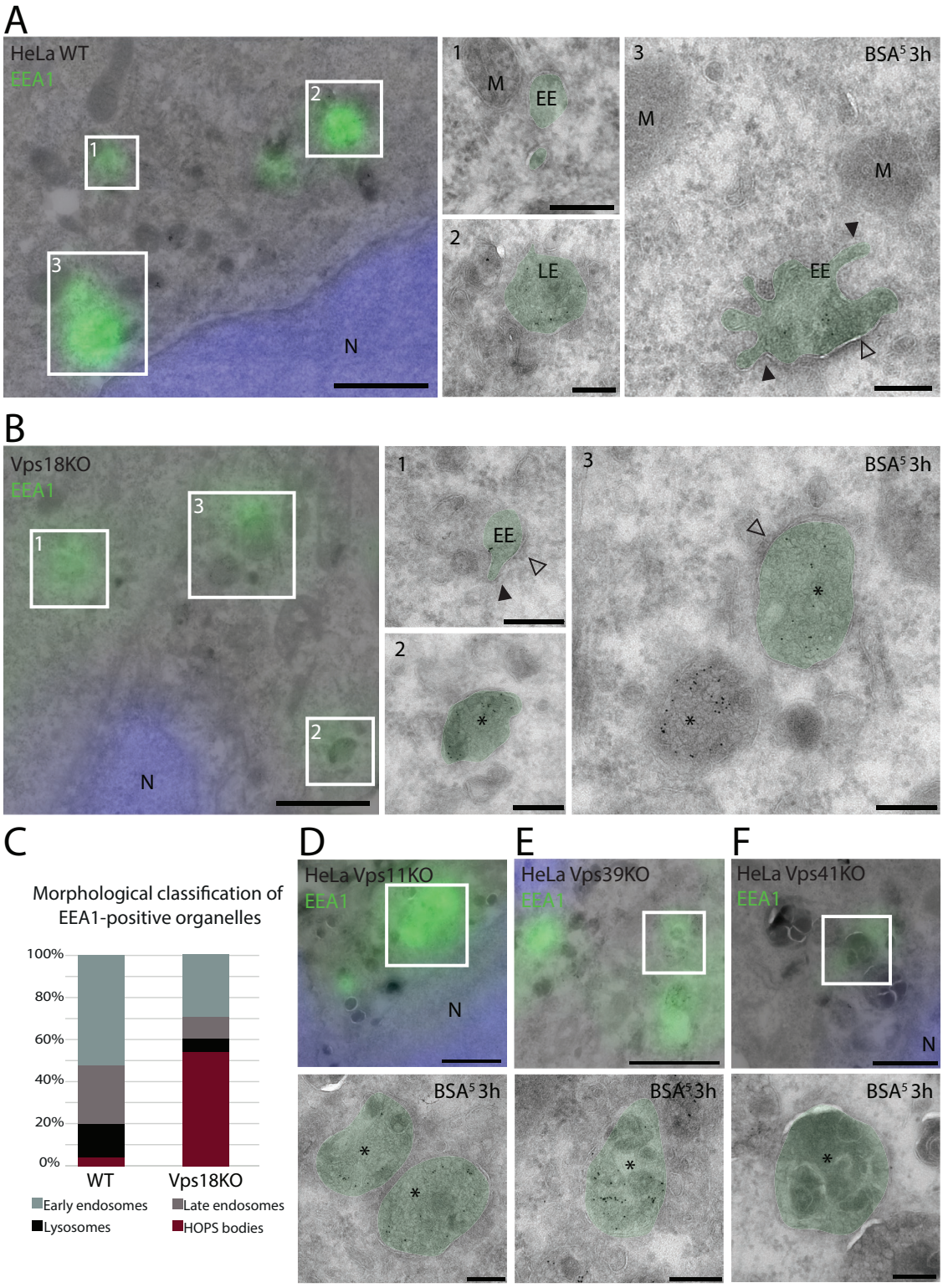


**FIGURE 7:** HOPS bodies display early and late ultrastructural characteristics. (A) CLEM of EEA1 in HeLa WT cells. EEA1 localizes to early (A1, A3) and late (A2) endosomes. Early endosomes were defined by their electron-lucent lumen, sorting tubules (closed arrows) and clathrin coats (open arrows). Late endosomes by numerous ILVs and dense content. (B) CLEM of EEA1 in Vps18 KO cells. EEA1 localizes to early endosomes (B1) and large, hybrid early-late endosomal compartments with heterogeneous content and clathrin coats (open arrow, B2, B3), that is, HOPS bodies (asterisks). (C) Classification of EEA1-positive organelles based on ultrastructure. In Vps18 KO cells, EEA1 label is highly enriched over HOPS bodies with hybrid early-late ultrastructure. $n = 25$ and 48 organelles for WT and Vps18 KO, respectively. (D–F) CLEM of EEA1 in HeLa Vps11 (D), Vps39 (E), and Vps41 (F) KO cells invariantly localizes EEA1 to HOPS bodies. *, HOPS bodies; EE, early endosome; M, mitochondrion; N, nucleus; LE, late endosome. 1 µm scale bars in CLEM overview, 200 nm in EM insets.

increase in endo-lysosomal organelles (Figure 8;Supplementary Figure S9). This prompted us to analyze the relative composition of the endo-lysosomal system for each condition. We randomly screened for ~200 endosomal compartments and classified these by morphology (Figure 8H). This revealed a minor relative decrease of early endosomes (39% in WT, 12–28% in HOPS KO cells) and lysosomes (49% in WT, 33–47% in HOPS KO cells) and a relative increase in late endosomes (4% in WT, 10–12% in HOPS KO cells). The fraction of HOPS bodies drastically increased in all HOPS KO cells (8% in WT, 29–41% in HOPS KO cells), confirming that accumulation of these organelles is specific for HOPS dysfunction (Figure 8H).

We also analyzed the distribution of endocytosed BSA$^5$. In WT cells, endocytosed BSA$^5$ was found in early and late endosomes as well as lysosomes. In HOPS KO cells, early and late endosomes and HOPS bodies were positive for BSA$^5$, but lysosomes were consistently negative (Figure 8I). The presence of endocytosed BSA$^5$ in HOPS bodies was consistent with the fluorescent data on internalized Dextran-AF488 (Figure 1C and D). The absence of BSA$^5$ from "classical" lysosomes confirmed previous EM studies in chemically fixed Vps41-silenced or -KO cells (Pols *et al.*, 2013a; van der Welle *et al.*, 2021).

Together, these EM data showed that all HOPS KO cells showed a striking increase in HOPS bodies, indicating that these organelles specifically accumulate upon HOPS dysfunction. HOPS bodies displayed a typical hybrid early–late endosomal morphology, which is in agreement with their hybrid early–late molecular composition (Figures 1 and 2). Interestingly, the BSA$^5$ uptake studies positioned early endosomes, late endosomes and HOPS bodies upstream of the HOPS dependent fusion step and lysosomes downstream. These data highlighted the role of HOPS as a determining factor for the transfer of endocytosed cargo from endosomes to lysosomes, while upstream of this transport step HOPS KO causes the accumulation of endosomes of hybrid early–late morphology.

### HOPS bodies contain p62/LC3-positive autophagic content

The current model of macroautophagy is that autophagosomes fuse directly with lysosomes to form autolysosomes, or with endosomes resulting in amphisomes that subsequently fuse with lysosomes (Yu *et al.*, 2018; Hu and Reggiori, 2022). These fusions have been reported to depend on the HOPS complex (Jiang *et al.*, 2014; Takáts *et al.*, 2014). Consistent with this, previous studies in HOPS depleted cells (van der Welle *et al.*, 2021; Terawaki *et al.*, 2023) showed increased levels of lipidated LC3 (LC3-II), the form of LC3 that is conjugated onto the autophagosomal membrane during macroautophagy. Higher levels of LC3-II are often interpreted as an increase in early autophagic compartments that are not (yet) fused with lysosomes. By Western blot, we confirmed the accumulation of LC3-II in all our HOPS KO cells, including those in A549 and HT1080 lines (Supplementary Fig. S10A). However, EM of HOPS KO cells did not reveal a marked increase in typical autophagosomes (Figure 8). Instead, we observed granules inside the HOPS bodies that were morphologically reminiscent to autophagic content accumulating in endo-lysosomes when cells are starved in the presence of the V-ATPase inhibitor Bafilomycin A1 (De Mazière *et al.*, 2022). These 100–250 nm sized, amorphous dense granules were frequently membrane-bound (Figures 7 and 8) and observed in all HOPS KO cells, both after HPF and chemical fixation. To establish or disprove the presence of autophagic content in HOPS bodies, we applied our recently optimized labeling protocol for LC3 and p62 immuno-EM (De Mazière *et al.*, 2022). This unequivocally localized p62 and LC3 in the lumen of HOPS bodies, in which they associated with the typical dense granules (Figure 9A and B, arrows). Of note, p62 and LC3 labeling was consistently absent from lysosomes, which – as shown above –also lacked internalized BSA$^5$ (Figure 8I).

We then performed immuno-EM of p62 combined with BSA$^5$ uptake (3 h), screened randomly for BSA$^5$-positive endosomes and established the percentage also labeled for p62. In WT control cells p62 is rapidly degraded in endo-lysosomal compartments and indeed <5% of BSA$^5$-positive endo-lysosomes contained p62 label. In contrast, in Vps41 KO cells most (60%, Figure 9D) BSA$^5$-positive compartments contained p62 and virtually all of these double-positive compartments were HOPS bodies. These data indicated that incorporation of autophagic cargo into HOPS bodies proceeded in the absence of HOPS. To investigate if this was dependent on macroautophagy we induced silencing of ATG7, a key protein for early stage autophagosome formation (Mizushima, 2020). By siRNA, we reached a depletion of ≥80% as measured by QPCR. This caused a striking increase in cytoplasmic patches of p62 in both HeLa WT and Vps41 KO cells (Figure 9C). Interestingly, despite the increase pf cytosolic p62, incorporation into HOPS bodies of Vps41 KO cells was strikingly reduced by depletion of ATG7 (from 60% in control siRNA to 41% in ATG7 siRNA, Figure 9C and D). These data indicated that the autophagic material in Vps41 KO endosomes at least in part derived from macroautophagy and implied that autophagosome-endosome fusion, that is, formation of amphisomes, proceeded in the absence of HOPS. To further investigate this, we depleted the autophagosomal SNAREs Syntaxin 17 or Ykt6, which are part of the same fusion machinery as the HOPS complex (Jiang *et al.*, 2014; Takáts *et al.*, 2014; ; Bas *et al.*, 2018; Takáts *et al.*, 2018). Depletion of these SNAREs in Vps41 KO cells did not decrease incorporation of p62 in BSA$^5$-positive compartments (Figure 9D; Supplementary Figure S10B). This further supported that macroautophagy of p62 into HOPS bodies could occur independent of the HOPS-Syntaxin 17-Ykt6 fusion complex.

Invagination of the endosomal membrane relies on the ESCRT complex (Vietri *et al.*, 2020). ESCRT-III has a major role in conventional ILV formation, but can also internalize cytosolic content marked by p62 for degradation in endo-lysosomes (Mejlvang *et al.*, 2018). This process is called microautophagy and relies on ESCRT components CHMP4B, Vps4A and Vps4B. Because HOPS bodies displayed typical bi-layered clathrin coats known to contain ESCRT components, we asked if microautophagy could contribute to the HOPS-independent uptake of p62 in HOPS bodies. In Vps41 KO cells depleted for CHMP4B or Vps4A/B; however, the HOPS bodies contained similar levels of p62 as in nondepleted cells (63% and 66% of BSA$^5$-positive organelles, Figure 9C and D). These data indicated that p62/autophagic content did not enter HOPS bodies through microautophagy (Figure 9C and D; Supplementary Figure S10B). Strikingly, Vps4A/B depletion led to an increase of p62 at the limiting membrane of HOPS bodies, indicative of lysophagy. Vps4A/B depletion also led to a dramatic cell death in Vps41 KO but not WT cells.

These data identified HOPS bodies as amphisomes. Incorporation of p62 and LC3 in HOPS bodies required ATG7-dependent autophagosome formation, but was independent of the HOPS-Syntaxin 17-Ykt6 complex for subsequent autophagosome–endosome fusion. In short, our results implied that amphisome formation, but not autolysosome formation, is independent of HOPS.

## DISCUSSION

In this paper, we addressed the role of the HOPS complex in the functional organization of the endo-lysosomal system. By generating HeLa KO cell lines for 4 different HOPS subunits, the class C core

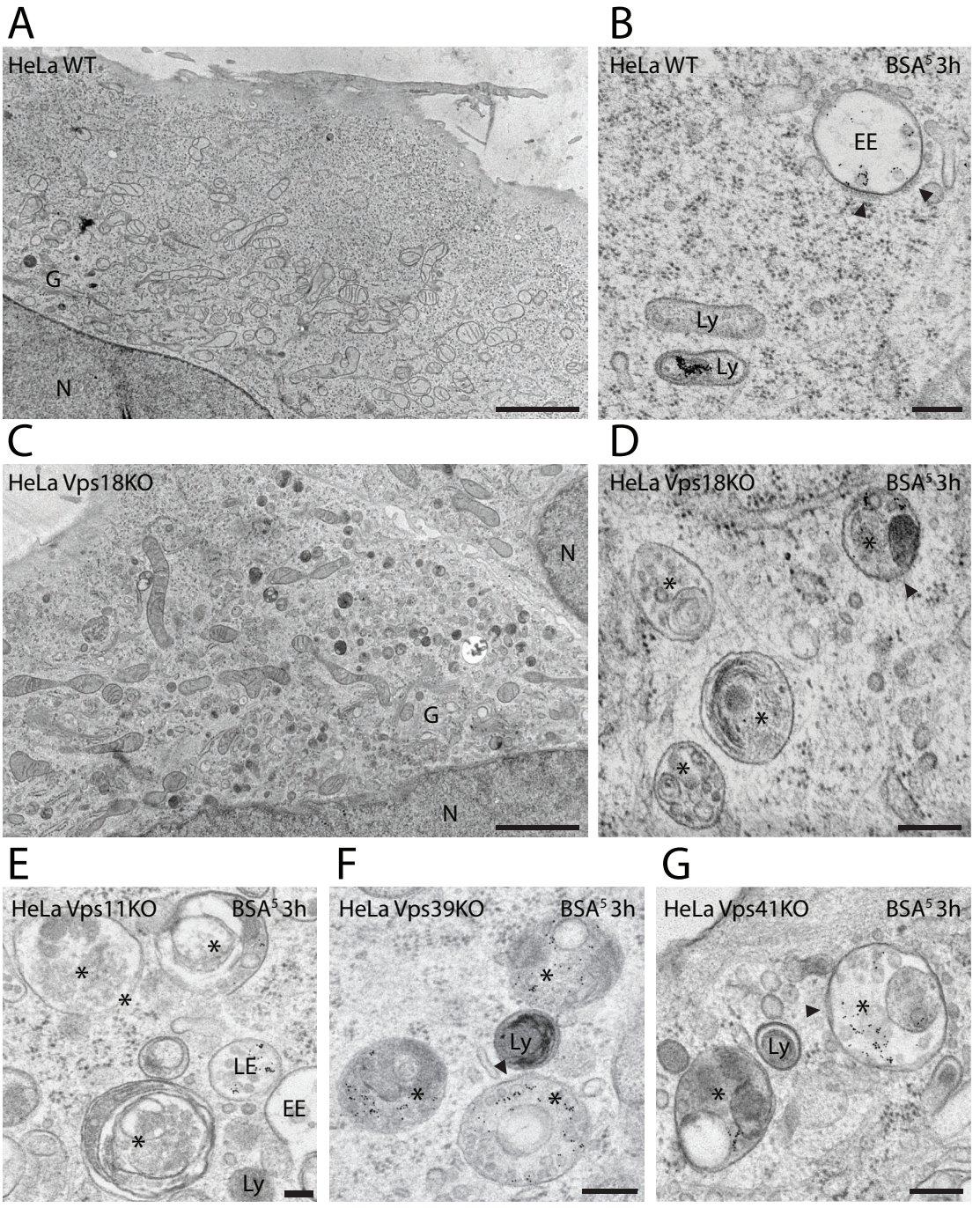
A
HeLa WT
G
N
B
HeLa WT
BSA5 3h
EE
Ly
Ly
C
HeLa Vps18KO
N
G
N
D
HeLa Vps18KO
BSA5 3h
E
HeLa Vps11KO
BSA5 3h
LE
EE
Ly
F
HeLa Vps39KO
BSA5 3h
Ly
G
HeLa Vps41KO
BSA5 3h
Ly
H Relative counts of endo-lysosomal organelles
100%
80%
60%
40%
20%
0%
WT
11KO
18KO
39KO
41KO
Early endosomes
Late endosomes
Lysosomes
HOPS bodies
I Percentage of organelles reached by BSA5
100%
80%
60%
40%
20%
0%
Early endosomes
Late endosomes
HOPS bodies
Lysosomes
WT
11KO
18KO
39KO
41KO

Vps11 and Vps18 and the HOPS-specific Vps39 and Vps41, we monitored the general defects of HOPS depletion. In all KO cell lines, we found a profound effect on prelysosomal compartments, as illustrated by increased colocalization of early (Rab5, PtdIns3P, EEA1) and late (Rab7, CD63, LAMP1, cathepsin D) endosomal markers (Figures 1 and 2; Supplementary Figures S1 and S2). By EM, HOPS KO cells showed an accumulation of morphologically hybrid compartments with ultrastructural characteristics of early (clathrin coats, recycling tubules) and late (ILVs, heterogenous content) endosomes (Figures 7 and 8; Supplementary Figures S8 and S9), to which we referred to as HOPS bodies. HOPS bodies were only mildly acidic (Figure 6C and D), were reached by endocytosed cargo (Figure 8) and unexpectedly also by autophagic proteins (Figure 9), which defined them as amphisomes. HOPS bodies also accumulated CI-MPR, the receptor for lysosomal enzymes that normally cycles between TGN and endosomes. CI-MPR failed to enter SNX1-positive retrograde recycling tubules originating from HOPS bodies, leading to receptor depletion from the TGN. Concomitantly, the levels of inactive pro-cathepsin D, a lysosomal hydrolase and substrate for CI-MPR, increased in the Golgi/TGN and in the medium (Figure 3; Supplementary Figures S3 and S5C). Cathepsin D that did reach HOPS bodies was not processed to its mature form and remained inactive. Together, these data show that loss of HOPS complex blocks or delays the transition of early to late endosomes, affects endosomal recycling properties and alters lysosomal enzyme trafficking and activation. Further, they suggest the existence of a HOPS-independent pathway for endosome-autophagosome fusion. Our findings are summarized in a model (Figure 10).

A striking phenotype of all HOPS KO cells was the accumulation of large, Rab5-Rab7–positive hybrid endosomes, the HOPS bodies (Figure 1, and E and F). The hybrid molecular make-up, increase in size, perinuclear localization, as well as the overall ultrastructure of these HOPS bodies resembled the endo-lysosomal phenotype of cells overexpressing constitutively active Rab5 (Rab5Q79L) (Wegener *et al.*, 2010), suggesting that lack of HOPS induced a defect in Rab5 to Rab7 conversion. Likewise, early studies in live cells have shown that depletion of the HOPS complex delays Rab5-to-Rab7 conversion (Rink *et al.*, 2005) and more recently others found that HOPS interacts with Rab5, Rab7, several of their effectors (Gillingham *et al.*, 2014; Van Der Kant *et al.*, 2015; Jongsma *et al.*, 2020) and the Mon1–Ccz1 complex, the Rab7 GEF required for Rab5 to Rab7 transition (Wang *et al.*, 2003; Poteryaev *et al.*, 2010). Based on these findings, it was suggested that subunits of the HOPS complex could act as a molecular platform for the Rab5-Rab7 conversion process. However, contradicting in vitro data showed that the HOPS complex is dispensable for Rab5 to Rab7 conversion (Langemeyer *et al.*, 2020). In our study, knock-out of any single subunit resulted in increased Rab5-Rab7 colocalization. This indirect readout for Rab5 to Rab7 conversion did not reveal the precise role of HOPS in this process. Nonetheless, it indicated that all subunits are required for normal Rab5 to Rab7 transition. If HOPS would act as a molecular platform for this conversion, we would have expected to see differences between the loss of specific subunits, with stronger effects for depletion of those subunits that facilitate key interactions. Based on our data, we consider it more probable that the role of HOPS in Rab5 to Rab7 conversion depends on membrane fusion activity of the full complex.

A surprising finding was the presence of p62 and LC3 in HOPS bodies (Figure 9), which defined them as amphisomes. Of note, expression of Orf3A, a protein encoded by SARS-CoV-2 that binds Vps39 and inactivates HOPS, also causes the accumulation of amphisomes (Miao *et al.*, 2021). Furthermore, accumulation of p62 in cells was noted after downregulation of Vps41 by exposure to Cadmium (Wang *et al.*, 2023). The accumulation of p62 in HOPS bodies is potentially relevant with respect to HOPS disease development (van der Beek *et al.*, 2019; Monfrini *et al.*, 2021b), since defects in p62-mediated proteostasis are linked to several types of neurodegenerative diseases (Kumar *et al.*, 2022). Both p62 and LC3 were, by immuno-EM, associated with typical dense granules indicative for the presence of autophagic cargo, as previously observed in cells treated with Bafilomycin A1 (De Mazière *et al.*, 2022). Because HOPS bodies were not or mildly acidic and only contained inactive pro-cathepsin D, the accumulation of p62- and LC3-marked autophagic cargo in their lumens is explained by this lack of degradative capacity. p62 and endocytosed BSA$^5$ were both found in HOPS bodies, but absent from lysosomes. Hence, in the absence of HOPS both endocytic and autophagic cargo reached endosomal compartments, but transfer to lysosomes was inhibited. Previously, using the same definitions for endosomes and lysosomes as here, we found that lysosomes are the major sites for hydrolase activity (Liv *et al.*, 2023). Altogether this suggests that HOPS is required for the transfer of endocytic and autophagic cargo from predominantly non-active endosomes to actively degrading lysosomes, signifying HOPS as an important gate keeper for lysosomal entry and cargo degradation.

The formation of amphisomes in HOPS KO cells implied that endosomal delivery of autophagic cargo proceeded in the absence of HOPS. Likewise, depletion of the SNAREs Syntaxin 17 or Ykt6, both implicated in HOPS-dependent autophagosome – endo-lysosome fusion (Lürick *et al.*, 2015; Matsui *et al.*, 2018; Takáts *et al.*, 2018), did not block entry of p62 in HOPS bodies (Figure 9C-D). This was unexpected since it has been reported that autophagic flux depends on the interaction between these autophagosomal SNAREs and the HOPS complex (Jiang *et al.*, 2014; Takáts *et al.*, 2014). Knockdowns of Vps4A/B or CHMP4B (Mejlvang *et al.*, 2018) in

**FIGURE 8:** HOPS KO induces accumulation of hybrid early – late endosomes, that is, HOPS bodies. HeLa WT and KO cells incubated with BSA$^5$ for 3 h were HPF fixed and embedded in EPON for EM imaging. (A, B) Overview of endocytic organelles in HeLa WT cells. Early endosomes (EE) show characteristic associated tubules and clathrin coats (arrowheads). Lysosomes (Ly) are small and dense and regularly positive for endocytosed BSA$^5$. (C, D) Vps18 KO cells. (C) Note the high abundance of endocytic compartments. (D) HOPS bodies (asterisks) appear as enlarged, BSA$^5$-positive endosomal organelles with hybrid early and late endo-lysosomal features: associated vesicles and tubules, clathrin coats (arrowheads), membrane whorls, dense content, numerous ILVs. (E–G) Examples of HOPS bodies (asterisks) in Vps11, Vps39 and Vps41 KO cells. Lysosomes are mostly negative for BSA$^5$. For more examples see Supplementary Figure S9. (H) Classification of endosomal organelles in HeLa WT and KO cells. HOPS bodies are strongly enriched in HOPS KO cells. n ≥ 200 organelles per condition. (I) Percentage of organelles containing BSA$^5$. BSA$^5$ reaches 67% of lysosomes in WT cells and only ~10% in HOPS KO cells. n ≥ 200 organelles per condition. *, Hybrid organelle; EE, early endosome; G, Golgi; N, nucleus; Ly, lysosome. Scale bars 2 µm (A, C), 200 nm (B, D–G).

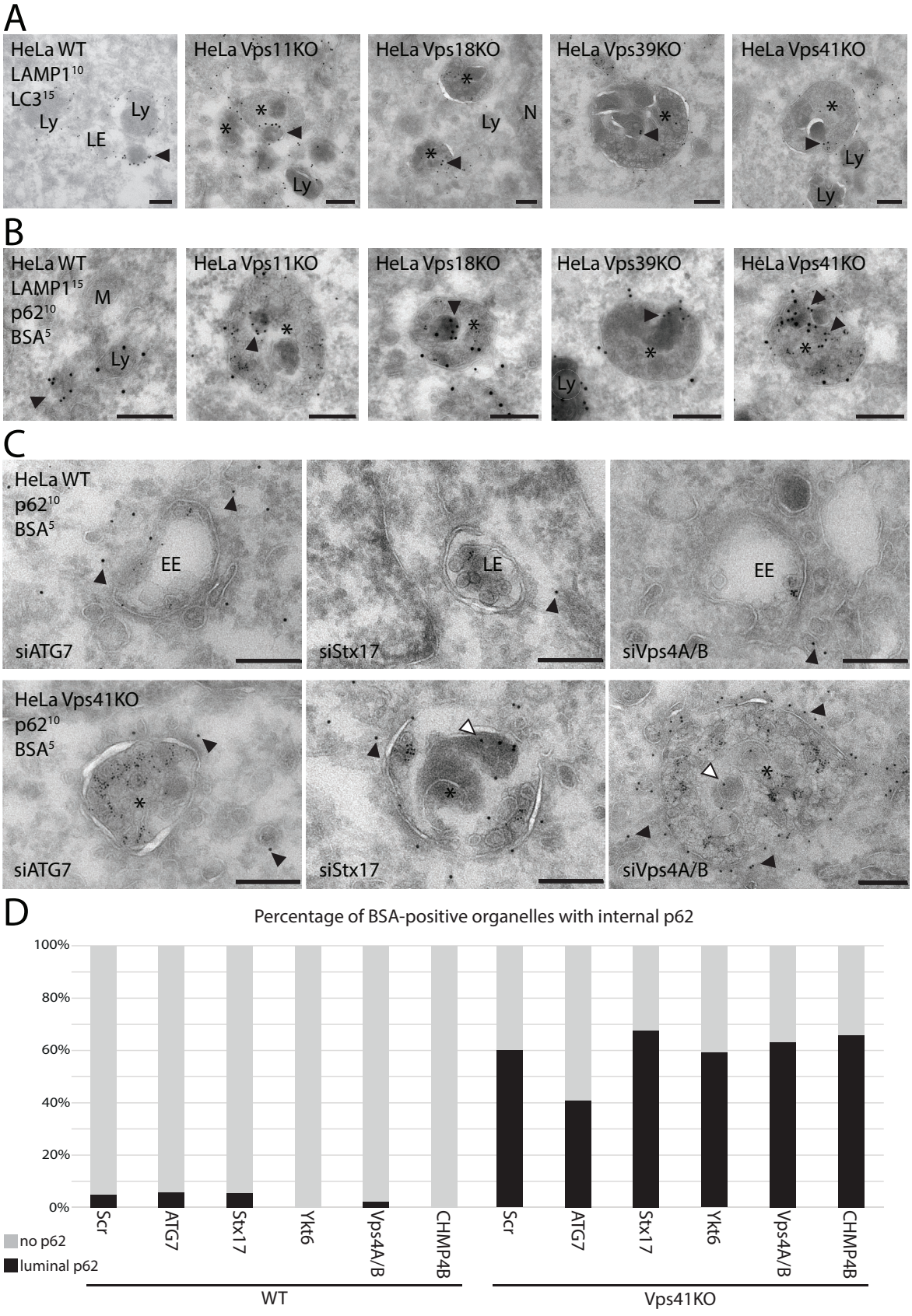


**FIGURE 9:** HOPS bodies contain autophagic materials. Cells were prepared for immuno-EM as in Figure 5. (A) Double immunogold labeling of LC3 (10 nm) and LAMP1 (15 nm). LC3 labels the typical dense structures (arrowheads) within LAMP1-positive HOPS bodies (asterisks). In WT cells, LC3 is sometimes seen on cytoplasmic granules (arrow), but not in endosomes. (B) Double labeling of p62 (10 nm) and LAMP1 (15 nm) in WT and HOPS KO cells. In WT cells, p62 label is

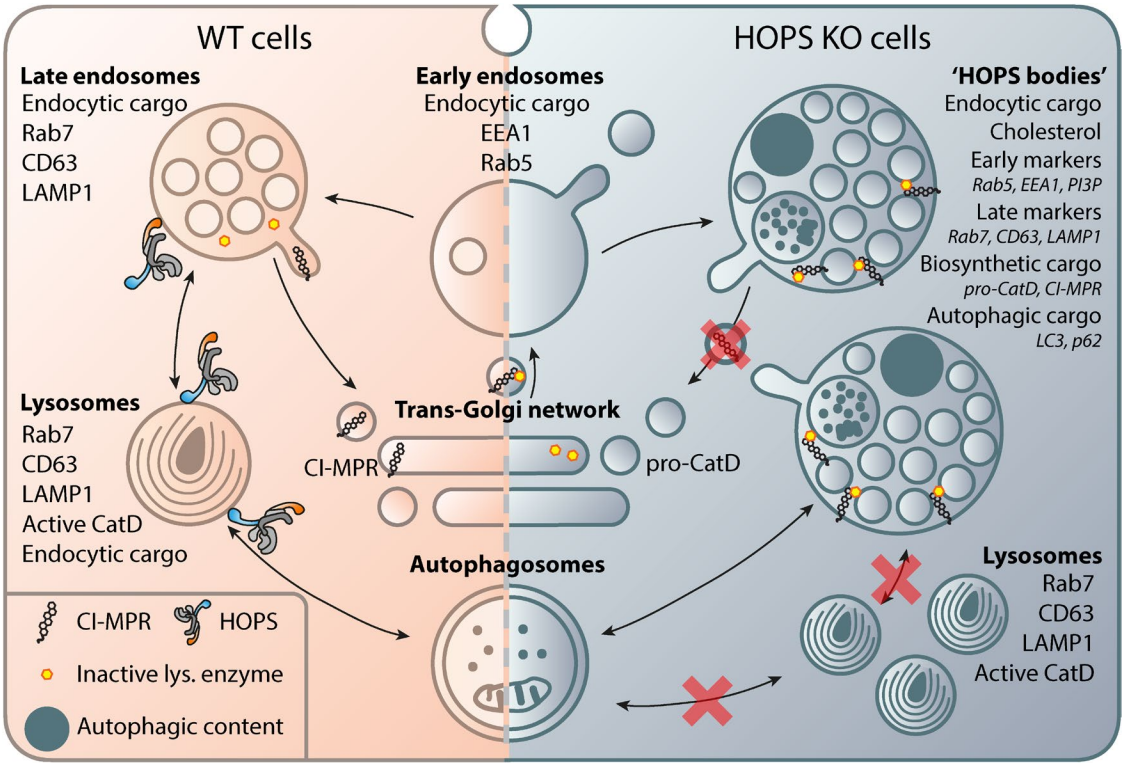


**FIGURE 10:** Summarizing model on the effects of HOPS depletion on the functional organization of the endo-lysosomal system. Loss of the HOPS complex causes accumulation of HOPS bodies, organelles of hybrid molecular and morphological composition. HOPS bodies are reached by endocytic and autophagic cargoes but fail to fuse with lysosomes. They have low enzymatic activity and are of neutral pH, which prevents degradation of endocytic and autophagic content in HOPS bodies, as well as the retrograde transport of CI-MPR to the Trans-Golgi network. Depletion of CI-MPR from TGN leads to local accumulation of pro-cathepsin D and a general increase in secretion of lysosomal hydrolases and autophagic content from HOPS bodies.

Vps41 KO cells excluded that uptake of p62 in HOPS bodies depended on microautophagy (Figure 9C and D). In contrast, depletion of ATG7–required for autophagosome formation–reduced the number of p62-positive endosomes from 60% to 41%. Together these data inferred that at least some of the autophagic cargo present in HOPS bodies derived from macroautophagy (Figure 9C and D), implying the existence of an alternative, HOPS-Stx17-Ykt6 independent mechanism of autophagosome –endosome fusion. The accumulation of HOPS bodies in HOPS KO cells is in line with the scenario that subsequent amphisome–lysosome fusion is HOPS dependent. Interestingly, the high numbers of HOPS bodies raise the question if autophagosome–endosome fusion normally prevails over autophagosome–lysosome fusion. Formation of amphisomes in control conditions may be obscured by rapid turnover of the amphisomes. The current literature on amphisome and autolysosome formation is rather ambiguous and clearly more work is required to address these questions (Reggiori and Ungermann, 2017; Ganesan and Cai, 2021; Hu and Reggiori, 2022).

Another unexpected finding was that depletion of the HOPS complex caused a redistribution of CI-MPR from the TGN to HOPS bodies (Figure 4). Depletion of CI-MPR from the TGN is known to increase secretion of lysosomal enzyme precursors (Meel and Klumperman, 2014), which was indeed the case for HOPS KO cells (Supplementary Figure S5C). Likewise, Anderson *et al.* recently reported a decrease in cellular CI-MPR levels in Vps39 or Vps41 KO cells and an increased secretion of CI-MPR ligand NPC2 (Anderson *et al.*, 2022). Lack of NPC2 causes an accumulation of endo-lysosomal cholesterol (Anderson *et al.*, 2022), this was supported by the lipid buildup we noticed in our EM studies (Figure 6) and was reported earlier (Swetha *et al.*, 2011). These and our present studies all indicate a trafficking defect for CI-MPR in HOPS KO cells. Since we observed that CI-MPR accumulated in HOPS bodies, we investigated if the SNX1-positive tubules of the retrograde ESCPE pathway were still formed. All our HOPS KO cell lines readily displayed SNX1-positive tubules by both IF and by immuno-EM (Figures 4A and B, 5, A–D; Supplementary Figure S6). In HOPS KO

only found in the cytoplasm (arrowhead). In HOPS KO cells, p62 is found in the HOPS bodies (asterisks) on similar structures as LC3 (arrowheads). (C) HeLa WT and Vps41 KO cells depleted for ATG7 (macroautophagy), Vps4A/B (microautophagy) or Stx17 (SNARE autophagosome–lysosome fusion) and labeled for p62 (10 n). Note accumulation of p62 on limiting membrane of HOPS bodies in Vps4A/B-depleted Vps41 KO cells, indicative of lysophagy. For more representative images and depletion conditions see Supplementary Figure S10B. (D) Quantification of the % $BSA^5$-positive organelles that contain p62 label. Only depletion of ATG7 reduces the amount of p62-positive HOPS bodies in Vps41 KO cells. >50 $BSA^5$-positive organelles were scored in each condition. EE, early endosome; N, nucleus; LE, late endosome; Ly, lysosome. Scale bars, 200 nm.

cells, however, these tubules were generally depleted from CI-MPR (Figure 5D), suggesting a block in the entry of CI-MPR into ESCPE tubules rather than a general block in recycling (Evans *et al.*, 2020; Simonetti *et al.*, 2023). In early studies it was shown that CI-MPR-ligand dissociation in acidifying endosomes is both necessary and sufficient to trigger recycling of CI-MPRs to the TGN (Brown *et al.*, 1986). Concomitantly, we found that inhibition of endosomal acidification by Chloroquine or Bafilomycin A1 relocalized CI-MPR from TGN to endosomes in HeLa WT cells. Interestingly, the drugs had no additional effect on CI-MPR redistribution in HOPS KO cells (Figure 6A and B). Moreover, by fluorescein pH measurements we found that HOPS bodies were not or only mildly acidified (Figure 6C and D). This lack of acidification is a plausible explanation for CI-MPR retention in the HOPS bodies and also explains why lysosomal enzymes in HOPS bodies are not processed to their active form (Figure 3). Of note, previous studies from our lab and others failed to find defects in CI-MPR and lysosomal enzyme transport after knockdown of HOPS subunits (Swetha *et al.*, 2011; Pols *et al.*, 2013a). Also, the "HOPS bodies" were not reported before, although we previously characterized Vps39 or Vps41-depleted cells by EM (Pols *et al.*, 2013a). The main difference between these and our present study is the use of genetic editing instead of siRNA-based silencing. From this we conclude that the accumulation of HOPS bodies and the endosomal trafficking defects occurs only after complete and long-term removal of HOPS complex activity. Altogether, we here showed that HOPS KO severely affected CI-MPR transport and thereby the trafficking and activation of lysosomal enzymes.

Interestingly, we did not find any obvious differences between the four different KO cell lines, even though Vps11 and Vps18 are also part of sister complex CORVET. This consistency in phenotypes was reported before (Wartosch *et al.*, 2015). Similarly, in a recent overview of CORVET and HOPS related diseases, we noticed that most pathological lesions caused by mutations in core components were related to the later stages of the endo-lysosomal system (van der Beek *et al.*, 2019). This makes it plausible that the phenotypes described in this study depend on assembly and activity of the full HOPS complex. We can, however, not rule out that depletion of individual subunits additionally affects specific subsets of endosomes or trafficking pathways, such as APPL1 endosomes or specific recycling pathways (Perini *et al.*, 2014; Jonker *et al.*, 2018), that were not investigated in this study.

The loss of endosome – lysosome fusion induced by HOPS KO cells does not easily explain the maturation, recycling and acidification defects in HOPS bodies, which occur upstream of lysosomes. A possible explanation is that the HOPS complex is also required for fusion of TGN-derived vesicles carrying lysosomal membrane proteins to late endosomes (Pols *et al.*, 2013b; Davis *et al.*, 2021). In yeast this pathway is known as the ALP pathway, which delivers lysosomal membrane proteins directly to the vacuole (Cowles *et al.*, 1997; Anand *et al.*, 2009; Llinares *et al.*, 2015). In *Drosophila*, a similar Vps41/Light–dependent TGN-derived pathway is important for lysosomal delivery of the membrane proteins LAMP1, NPC1, and the V-ATPase (Swetha *et al.*, 2011). Indeed, we found small vesicles accumulating around the HOPS bodies in Vps41 KO cells (Figure 8G; Supplementary Figure S9E), which were morphologically reminiscent of the TGN-derived LAMP carriers previously identified in Vps41 and VAMP7 knockdown cells (Pols *et al.*, 2013b; Davis *et al.*, 2021), and positive for LAMP1 by immuno-EM (Pols *et al.*, 2013b). A lack in the delivery of lysosomal membrane proteins could directly and indirectly affect endosomal maturation, for example by altering recruitment of phosphoinositides or effector proteins, by altering cholesterol processing and egress from endosomes, changing pH or ionic balance, and by activation of lysosomal hydrolases (Huotari and Helenius, 2011). Further experimentation is required to investigate and proof this hypothesis. Interestingly, HOPS KO cells still contained active, acidified lysosomes (Wartosch *et al.*, 2015; van der Welle *et al.*, 2021), albeit that these were not reached by endocytosed and autophagic cargo in our experimental conditions. In fact, HOPS KO cells showed a general increase in endo-lysosomal compartments (Figure 8H), which is likely explained by nuclear translocation of TFE3/TFEB and consequent activation of the CLEAR network (van der Welle *et al.*, 2021). These observations might also explain why some studies report an effect on hydrolase activity after HOPS depletion, for example in *D. melanogaster car*/Vps33A or *dor*/Vps18 mutants and Vps18 conditional KO mice (Sriram *et al.*, 2003; Peng *et al.*, 2012), while others do not (Swetha *et al.*, 2011; Graham *et al.*, 2013; Pols *et al.*, 2013b; van der Welle *et al.*, 2021;). How and by which kinetics lysosomes in HOPS KO cells are formed and how they might differ from lysosomes in WT cells remains a topic for future studies.

Summarizing, our data show that HOPS complex is required for endosomal maturation prior to the stage of endo-lysosomal fusion and reveal a central role of the HOPS tethering complex in orchestrating the endo-lysosomal system, including endosomal recycling pathways and autophagic clearance. Moreover, we provide evidence for a HOPS-independent pathway for incorporation of autophagic material into endosomes, which evokes further investigation into the role and mechanism of amphisome formation.

## MATERIALS AND METHODS

**Request a protocol through *Bio-protocol*.**

### Antibodies and reagents

For antibodies used in this study, see (Table 1), effectene transfection reagent (301425, QIAGEN) and HiPerFect transfection reagents (301704, QIAGEN) were used. SiRlysosome (SC012, Spirochrome), Dextran-AF488 (D22910, Thermo Fisher Scientific) and Dextran-fluorescein (D1820, Thermo Fisher Scientific) were used in fluorescence microscopy. The following siRNAs were used: All stars negative control siRNA (1027281, QIAGEN), CHMP4B Smartpool (L-018075-01-0005, Horizon Discovery), Stx17 Smartpool (M-020965-01-0005, Horizon Discovery), ATG7 Smartpool (L-020112-00-0005, Horizon Discovery), Ykt6 siRNA directed against sense 5′-ATTCATTGTCAGCAATGACCACACC-3′ (Matsui *et al.*, 2018), Vps4A siRNA directed against sense 5′-CTGTGGTTTGCATGTCGGA-3′ (Mejlvang *et al.*, 2018), Vps4B siRNA directed against sense 5′-CCAAAGAAGCACTGAAAGA-3′ (Mejlvang *et al.*, 2018). The 2xFYVE-mCherry construct was ordered from AddGene (deposited by Harald Stenmark, 140050). The EEA1-mCherry construct was ordered from AddGene (deposited by Yusuke Ohba, #174452). The EEA1-mCherry fragment from this vector was cloned into a pmini-Tol2 expression vector (original deposited on AddGene by Stephen Ekker, #31829, we obtained a modified backbone with EF1α promotor from Jooske Monster, CMM, UMCU) using restriction-ligation. Vector with Transposase from *Oryzias latipes* was obtained from Jooske Monster, CMM, UMCU.

### Cell lines

HeLa parental cells were obtained from DSMZ (ACC 57), Vps11, Vps18, Vps39 and Vps41 knock-outs were generated as described previously (van der Welle *et al.*, 2021). The A549 HOPS KO cell lines were obtained using gRNA sequence 5′-AGTGGGGGATGCCCACGCTA-3′ for Vps18 and gRNA sequence 5′-AAGTATTTCAGTTACCCCAT-3′ for Vps41. For HOPS KO in HT1080 cell lines, we used gRNA sequence 5′-GCGAGTTCTCGTACTCATCC-3′ for Vps18

| Name | Host | Catalog number | Company | Dilutions |
|---|---|---|---|---|
| LAMP1 | Mse | 555798 | BD Pharmingen | 1:500 (IF) |
| cathepsin D | Gt | AF1014 | R&D Systems | 1:500 (IF), 1:1000 (WB) |
| cathepsin B | Gt | AF953 | R&D Systems | 1:1000 (WB) |
| Calnexin | Rb | Ab22595 | Abcam | 1:1000 (WB) |
| Rab5 | Mse | 610725 | BD Biosciences | 1:250 (IF) |
| Rab7 | Rb | 9367 | Cell Signaling Technology | 1:250 (IF) |
| Vps11 | Rb | ab170869 | Abcam | 1:500 (WB) |
| Vps18 | Rb | ab178416 | Abcam | 1:500 (WB) |
| Vps41 | Mse | sc-377118 | Santa Cruz Biotechnology | 1:1000 (WB) |
| CD63 | Mse | H5C6 | DSHB | 1:500 (IF) |
| EEA1 | Mse | 610457 | BD Transduction | 1:250 (IF), 1:150 (CLEM) |
| EEA1 | Rb | C45B10 | Cell Signaling Technology | 1:250 (IF) |
| Vps35 | Gt | Ab10099 | Abcam | 1:500 (IF) |
| CI-MPR | Rb | Kind gift from A. Hille/K. von Figura | | 1:300 (IF), 1:50 (EM) |
| CI-MPR | Rb | Kind gift from S. Kornfeld | | 1:1000 (WB) |
| SNX1 | Rb | Kind gift from P. Cullen | | 1:150 (EM) |
| SNX1 | Mse | 611482 | BD Biosciences | 1:250 (IF) |
| TGN46 | Shp | AHP500 | Bio-Rad (Serotec) | 1:500 (IF) |
| GM130 | Mse | Kind gift from E. Sztul | | 1:250 (IF) |
| p62 | Mse | 610833 | BD Biosciences | 1:1000 (WB) |
| p62 | GnP | GP62-C | Sanbio | 1:100 (EM) |
| LC3 | Mse | CTB-LC3-2-IC | Cosmo Bio | 1:10 (EM) |
| AF488 anti-mouse | Dk | A21202 | Life Technologies | 1:250 (IF) |
| AF568 anti-rabbit | Dk | A10042 | Life Technologies | 1:250 (IF) |
| AF647 anti-goat | Dk | A21447 | Life Technologies | 1:250 (IF) |
| AF488 anti-goat | Dk | A11055 | Life Technologies | 1:250 (IF) |
| AF555 plus anti-mouse | Dk | A32773 | Thermo Fisher Scientific | 1:250 (IF) |
| Anti-mouse | Rb | 610-4120 | Rockland | 1:300 (EM) |

**TABLE 1:** The following antibodies were used in this manuscript.

and gRNA sequence 5′-GCCAGACAGTCGATTTGCAG-3′ for Vps39. The lines were validated by Western blot (Supplementary Figure S4, A and B), or for Vps39 by genomic DNA isolation and sequencing (Supplementary Figure S4C), which revealed a single base deletion at the expected cut site for both alleles.

EEA1-mCherry–expressing cell lines were obtained by cloning EEA1-mCherry into a minitol vector designed for stable expression under an EF-1α promotor. HeLa WT, Vps18, and Vps39 KO lines were transfected with this vector and a vector expressing a transposase. After 48 h, puromycin was added to the medium at 1 µg/ml for selection of cells that had the minitol vector stably integrated.

### Cell culture and transfection

HeLa, A549, and HT1080 cells and CRISPR/Cas9 KO lines were cultured in DMEM supplemented with 20% FCS and penicillin and streptomycin. They were incubated in 37°C, 5% $CO_2$ incubators, passaged twice per week on average, and kept in culture until passage 20. For transfection of cells using plasmids, cells were incubated with effectene and plasmid mix ON and given normal medium 4 h before fixation or imaging. For knock-down of cells, we used HiPerfect and siRNAs at 20 nM end concentration. The HiPerfect mix was added to culture medium. After 72 h, cells were treated again with siRNAs for another 72 h before use in experiments. The efficiency of the knock-down was validated by QPCR and ≥80% reduction was obtained for all experiments used in this study.

### Dextran uptake assay

Cells were incubated with SiRlysosome (SC012, Spirochrome), 1:1000 in normal DMEM medium for 60 min. Then dextran-AF488 was added to the SiRlysosome-medium at final concentration 0.2 mg/ml, incubated for 2 h, washed five times with fresh, 37°C DMEM, and fixed in 4% FA. If needed, additional IF staining was performed using the protocol described below, otherwise the sample was washed three times in PBS, once in $H_2O$ and mounted using ProLong Dapi Diamond (P36962, Thermo Fisher Scientific). Slides were imaged within 3 d after fixation.

### Western blotting

For analysis of whole-cell lysates by Western blot, cells were cultured in standard cell culture plates, placed on ice, washed with ice-cold PBS, and scraped and lysed in 1% CHAPS lysis buffer. The samples were spun down at ≥10,000 × *g* for 10 min at 4°C to remove

cellular debris and equalized using a Bradford protein assay (Bio-Rad). SDS sample buffer was added, samples were run on precast 4–20% gradient gels (Bio-Rad) and transferred to Mini PVDF membranes (Bio-Rad) using the Trans-Blot TurboTransfer system (Bio-Rad). The membranes were blocked in Odyssey PBS Blocking buffer (LI-COR) at room temperature for 1 h and then incubated with primary antibodies in 0.1% TBST overnight at 4°C. Membranes were washed in 0.1% TBST and incubated with secondary antibodies for 1 h at room temperature before being washed in 0.1% TBST, followed by PBS and then $H_2O$. Membranes were scanned on an Amersham Typhoon Laser scanner (GE Healthcare).

For analysis of culture medium, cells were cultured in 15-cm dishes and incubated with serum-free medium overnight. The medium was collected, spun at 100,000 × *g* to remove any debris or particles, and the supernatant was precipitated by adding 10% trichloroacetic acid (TCA). The mixture was placed on ice for 30 min and then spun down at 10,000 × *g* at 4°C for 15 min. The supernatant was aspirated and washed with acetone at 4°C. The dry pellet was then resuspended in SDS buffer and Western blotting was performed as described above. For loading control, the corresponding cells from the 15-cm dish were processed as described above, with the exception that they were not equalized. The protein concentration in these samples therefore reflects the number of cells in the dish.

### Immunofluorescence staining

Cells were prepared for IF staining by seeding on glass coverslips and fixation with 4% FA for 15–20 min. The coverslips were washed with PBS three times, permeabilized in 0.1% TritonX-100 for 10 min at room temperature, and blocked in 1% BSA in PBS for 10 min at room temperature. Coverslips were incubated with primary antibodies diluted in 1% BSA for 1 h at room temperature followed by three PBS washes and incubation with secondary antibodies for 30 min at room temperature. Coverslips were then washed three times with PBS, once in $H_2O$, and mounted on glass slides using ProLong DAPI Diamond (P36962, Thermo Fisher Scientific).

Slides were imaged at room temperature using a Leica Thunder microscope with 100×, 1.47 NA TIRF oil objective or a DeltaVision with 100×, 1.40 NA oil objective. For confocal imaging, slides were imaged on a Zeiss LSM 700 with 63×, 1.40 NA oil objective at room temperature.

### pH measurements

The pH measurements were performed as described by Canton and Grinstein (Canton and Grinstein, 2015). To obtain a calibration dataset, HeLa WT cells were incubated with 0.2 mg/ml Dextran-fluorescein in normal medium for 3 h, washed four times with culture medium, and incubated in a pH-buffered solution containing 140 mM KCl, 1 mM $MgCl_2$, 1 mM CaCl, 5 mM glucose, and 25 mM of acetate-acetic acid, MES or HEPES buffer, depending on the desired pH. Immediately before imaging, Nigericin was added to an end concentration of 10 µM to equalize endo-lysosomal pH to the buffered pH. Cells were then imaged with 440 and 480 excitation and a fluorescein emission filter on a Leica Thunder microscope with 100×, 1.40 NA oil objective and 37°C, 5% $CO_2$ live-cell imaging chamber. Emission ratios of fluorescein 440/480 excitation channels were obtained for seven samples buffered in a range from pH 4 to pH 8. A sigmoid curve was fitted to describe the relation of fluorescein ratio and pH, which was used to calculate pH from the live-cell measurements subsequently taken (Supplementary Figure S7). We benchmarked our calibration by live-cell imaging and measuring the average pH of 3-h uptake Dextran-fluorescein–positive compartments in HeLa WT cells, which returned an expected acidified pH of 5.1 (Supplementary Figure S7, C and D). Continuing, HeLa WT, Vps18, and Vps39 KO cells stably expressing EEA1-mCherry were incubated with 0.2 mg/ml Dextran-fluorescein for 3 h, washed four times and imaged in phenol-red free, otherwise normal culture medium. Samples were then imaged on a Leica Thunder microscope. The emission ratios of fluorescein 440/480 excitation channels were obtained on a per-compartment basis for >10 cells. Analysis of compartment intensity and ratios was performed in FIJI using a custom macro. The formula from the sigmoid curve fitted to the calibration samples was used to calculate pH values from the emission ratios of fluorescein 440/480 excitation.

### Image analysis

Light microscopy images were analyzed using FIJI (Schindelin *et al.*, 2012). The ComDet Plug-In (Eugene Katrukha, Cell Biology, Utrecht University) was used for spot detection, spot size quantification, spot intensity measurements and colocalization analysis. EEA1 and CI-MPR colocalization was measured as the percentage of overlap between thresholded signal masks of the two channels. All measurements were performed per cell in a custom cell-segmenting macro.

For quantification of CLEM data, organelles were selected based on the presence of fluorescent EEA1 signal and categorized based on morphological characteristics described below.

Morphological analysis of the HPF samples was done by random selection of ~200 endocytic organelles per condition. Multiple characteristics were measured for each organelle, which were then categorized on the basis of morphological characteristics described below.

For quantification of p62-positive content in endosomal organelles (Figure 9D), ~50 $BSA^5$-positive organelles were imaged for each condition and scored for the number of gold particles representing p62. Organelles with 0 particles were regarded as negative, organelles with 1 particle were excluded, and organelles with >1 particle were considered p62-positive.

### EM of resin-embedded, high-pressure frozen cells

Cells were seeded on sapphire disks for 24 h and incubated with $BSA^5$ for 3 h before HPF. 10 min before HPF, cells were washed with full DMEM. The sapphire disks and cells were transferred into sample holders and inserted into a Leica EM ICE (Leica Microsystems) and frozen. After freezing, the samples were stored in $LN_2$. Samples were freeze substituted with chemical fixative and postfixed in 2% $OsO_4$. Cells were further processed in EPON in increasing concentrations and finally embedded in 100% EPON, polymerized for 3 d at 60°C.

Resin embedded cells were prepared for thin sectioning by removal of the sapphire disk and trimming of the stub to a rectangle of ~0.5 by 1 µm. 60–70 nm Sections were made on a Leica Ultracut S (Leica microsystems) using a DiATOME Ultra Diamond Knife 45°. Sections were deposited on Formvar- and carbon-coated copper grids and poststained using uranyl and lead citrate in a Leica EM AC20 (Leica microsystems). Samples were imaged on a Tecnai T12 (FEI Tecnai) transmission electron microscope (TEM) using SerialEM software (Mastronarde, 2018). Image tileset stitching was done with Etomo EM processing software (Mastronarde and Held, 2017).

### On-section CLEM

A detailed protocol for this procedure is available in van der Beek *et al.* (van der Beek *et al.*, 2022, 2023) Briefly, cells were fixed with 4% FA overnight, washed, and scraped before being pelleted and

embedded in 12% (wt/vol) gelatin. Embedded cell pellets were cut into smaller (0.5 $mm^3$) blocks, mounted on aluminum pins and snap frozen in LN2.

Frozen samples were trimmed and sectioned to 90-100 nm on a Leica UC7 Cryo Microtome using a DiATOME Cryo Diamond Knife 45°. The sections were picked up using a 1:1 mixture of 2.3M sucrose and 1.8% methylcellulose and deposited on Formvar- and carbon-coated copper grids. Grids were incubated in PBS at 37°C for 30 min, washed with PBS 0.15% glycine, blocked in PBS with BSA-c and fish-skin gelatin, and incubated with primary antibodies for 1 h at room temperature. The grids were then washed and incubated with fluorescent secondary antibodies for 30 min at room temperature. After further washes, grids were sandwiched between clean slideglasses and coverslips in 50% Glycerol and imaged on a Leica Thunder widefield microscope using a 100×, 1.47 NA TIRF objective at room temperature. After acquisition of an image tileset of the sections, the grids were retrieved from the slideglass, washed, and stained using Uranyl Acetate. The grids were then imaged in a Tecnai T12 TEM (FEI Tecnai) using SerialEM, selecting areas based on fluorescence microscopy. Image tilesets of the selected areas were generated at 42,000×, stitched together in Etomo postprocessing software and correlated with the fluorescence data (Paul-Gilloteaux *et al.*, 2017).

### IF on sections

Samples and sections were obtained as under "On-section CLEM" above, except that 150-nm sections were obtained and they were deposited on 10-mm coverslips. They were processed in the same manner as CLEM samples up to secondary antibody incubation, after which they were washed and mounted on slideglasses using ProLong DAPI Diamond (P36962, Thermo Fisher Scientific). They were imaged as described under "Immunofluorescence staining".

### Immuno-EM

Immunogold labeling of thawed cryosections was performed as developed and optimized in our lab, for details see (Slot and Geuze, 2007; De Mazière *et al.*, 2022). The procedure follows the protocol for CLEM up to and including sectioning. After sectioning, grids were placed on PBS at 37°C for 30 min, washed with PBS 0.15% glycine, blocked in PBS with BSA-c and fish-skin gelatin, and labeled with primary antibodies for 1 h at room temperature. Grids were washed, incubated with a bridging rabbit anti-mouse antibody for 20 min at room temperature, washed again, and incubated with Protein A coupled to 10 or 15 nm gold (PAG) particles for 20 min at room temperature. In case of double labeling, the grids were fixed in 1% GA for 5 min after the first labeling, washed, and then the labeling was repeated with a second primary antibody. After PAG labeling, grids were washed extensively in $H_2O$ before staining with Uranyl Acetate. Immuno-EM samples were imaged on a Tecnai T12 TEM or Tecnai T20 (FEI Tecnai) using SerialEM or Radius image acquisition software.

### Morphological definitions of the endo-lysosomal system

The EM morphology of the endo-lysosomal system has been studied for many decades. Immunogold labeling and functional assays have elucidated key structure–function relationships that are generally applied to categorize the different endo-lysosomal subtypes (Raiborg *et al.*, 2002; Mari *et al.*, 2008; Eskelinen *et al.*, 2011; Klumperman and Raposo, 2014; Fermie *et al.*, 2018; Davis *et al.*, 2021; Barral *et al.*, 2022; van der Beek *et al.*, 2022; ). Based on these collective findings, we used the following definitions for morphological definition of distinct endo-lysosomal organelles. Although these definitions are not absolute, they allow us to interpret ultrastructural findings and changes in a nonarbitrary way.

Early endosomes: largely electron-lucent organelles with <6 ILVs, frequently displaying flat, bi-layered clathrin coats on their limiting membrane and forming tubular extensions. Late endosomes: rounded shape, lumen-containing medium electron-dense content and >5 ILVs. Lysosomes: vacuoles of variable size and shape, amorphous content ranging from electron lucent to highly electron-dense, ILVs, and onion-like concentric rings of membranes. HOPS bodies displayed both early and late endosomal features as clathrin coats, associated tubules, ILVs, membranes, and amorphous and regularly dense granules, sometimes surrounded by a membrane, indicative of autophagic cargos. Some of these features are also displayed by late endosomes and (auto)lysosomes in WT cells, which is why our control cells contained low, but nonzero numbers of "HOPS bodies".

## ACKNOWLEDGMENTS

We thank our colleagues from the Center for Molecular Medicine and especially Catherine Rabouille of the Hubrecht Laboratory for fruitful discussions and feedback. We thank Matteo for support and advice on some of the experiments. We warmly thank Bas van Zuijlen, Susan Zwakenberg, and Fried Zwartkruis for help with generating knock-out cell lines. N.L. is supported by a ZonMw TOP grant (40-00812-98-16006 to J.K.). P.S. is supported by a DFG grant (FOR2625 to J.K. as part of the Research Consortium). The EM infrastructure used in this work is part of the Netherlands Electron Microscopy Infrastructure (NEMI), a research program National Roadmap for Large-Scale Research Infrastructure, which is financed by the Dutch Research Council to J.K. (project number 184.034.014).

## REFERENCES

Anand VC, Daboussi L, Lorenz TC, Payne GS (2009). Genome-wide analysis of AP-3–dependent protein transport in yeast. Mol Biol Cell 20, 1592–1604.

Anderson J, Walker G, Pu J (2022). BORC-ARL8-HOPS ensemble is required for lysosomal cholesterol egress through NPC2. Mol Biol Cell 33, ar81.

Baker RW, Jeffrey PD, Zick M, Phillips BP, Wickner WT, Hughson FM (2015). A direct role for the Sec1/Munc18-family protein Vps33 as a template for SNARE assembly. Science 349, 1111–1114.

Balderhaar HJK, Ungermann C (2013). CORVET and HOPS tethering complexes - coordinators of endosome and lysosome fusion. J Cell Sci 126, 1307–1316.

Ballabio A, Bonifacino JS (2020). Lysosomes as dynamic regulators of cell and organismal homeostasis. Nat Rev Mol Cell Biol 21, 101–118.

Barral DC, Staiano L, Guimas Almeida C, Cutler DF, Eden ER, Futter CE, Galione A, Marques ARA, Medina DL, Napolitano G, *et al.* (2022). Current methods to analyze lysosome morphology, positioning, motility and function. Traffic 23, 238.

Bas L, Papinski D, Licheva M, Torggler R, Rohringer S, Schuschnig M, Kraft C (2018). Reconstitution reveals Ykt6 as the autophagosomal SNARE in autophagosome-vacuole fusion. J Cell Biol 217, 3656–3669.

Bowman EJ, Siebers A, Altendorf K (1988). Bafilomycins; A class of inhibitors of membrane ATPases from microorganisms, animal cells, and plant cells. Proc Natl Acad Sci USA 85, 7972–7976.

Braulke T, Bonifacino JS (2009). Sorting of lysosomal proteins. Biochim Biophys Acta 1793, 605–614.

Brocker C, Kuhlee A, Gatsogiannis C, Kleine Balderhaar HJ, Honscher C, Engelbrecht-Vandre S, Ungermann C, Raunser S (2012). Molecular architecture of the multisubunit homotypic fusion and vacuole protein sorting (HOPS) tethering complex. Proc Natl Acad Sci USA 109, 1991–1996.

Brown WJ, Constantinescu E, Farquhar MG (1984). Redistribution of mannose-6-phosphate receptors induced by tunicamycin and chloroquine. J Cell Biol 99, 320–326.

Brown WJ, Farquhar MG (1984). The mannose-6-phosphate receptor for lysosomal enzymes is concentrated in cis Golgi cisternae. Cell 36, 295–307.

Brown WJ, Goodhouse J, Farquhar MG (1986). Mannose-6-phosphate receptors for lysosomal enzymes cycle between the Golgi complex and endosomes. J Cell Biol 103, 1235–1247.

Burd C, Cullen PJ (2014). Retromer: a master conductor of endosome sorting. Cold Spring Harb Perspect Biol 6, a016774 .
Canton J, Grinstein S (2015). Measuring lysosomal pH by fluorescence microscopy. Methods Cell Biol 126, 85–99.
Chou HT, Dukovski D, Chambers MG, Reinisch KM, Walz T (2016). CATCHR, HOPS and CORVET tethering complexes share a similar architecture. Nat Struct Mol Biol 23, 761–763.
Collins KM, Thorngren NL, Fratti RA, Wickner WT (2005). Sec17p and HOPS, in distinct SNARE complexes, mediate SNARE complex disruption or assembly for fusion. EMBO J 24, 1775–1786.
Collins KM, Wickner WT (2007). trans-SNARE complex assembly and yeast vacuole membrane fusion. Proc Natl Acad Sci USA 104, 8755–8760.
Cowles CR, Snyder WB, Burd CG, Emr SD (1997). Novel Golgi to vacuole delivery pathway in yeast: Identification of a sorting determinant and required transport component. EMBO J 16, 2769–2782.
D'Agostino M, Risselada HJ, Lürick A, Ungermann C, Mayer A (2017). A tethering complex drives the terminal stage of SNARE-dependent membrane fusion. Nature 551, 634–638.
Davis LJ, Bright NA, Edgar JR, Parkinson MDJ, Wartosch L, Mantell J, Peden AA, Luzio JP (2021). Organelle tethering, pore formation and SNARE compensation in the late endocytic pathway. J Cell Sci 134, jcs255463. doi:10.1242/jcs.255463.
Delevoye C, Marks MS, Raposo G (2019). Lysosome-related organelles as functional adaptations of the endolysosomal system. Curr Opin Cell Biol 59, 147–158.
De Mazière A, van der Beek J, van Dijk S, de Heus C, Reggiori F, Koike M, Klumperman J (2022). An optimized protocol for immuno-electron microscopy of endogenous LC3. Autophagy 18, 3004–3022.
Eskelinen EL, Reggiori F, Baba M, Kovács AL, Seglen PO (2011). Seeing is believing: The impact of electron microscopy on autophagy research. Autophagy 7, 935–956.
Evans AJ, Daly JL, Anuar ANK, Simonetti B, Cullen PJ (2020). Acute inactivation of retromer and ESCPE-1 leads to time-resolved defects in endosomal cargo sorting. J Cell Sci 133, jcs246033.
Fermie J, Liv N, ten Brink C, van Donselaar EG, Müller WH, Schieber NL, Schwab Y, Gerritsen HC, Klumperman J (2018). Single organelle dynamics linked to 3D structure by correlative live-cell imaging and 3D electron microscopy. Traffic 19, 354–369.
Ganesan D, Cai Q (2021). Understanding amphisomes. Biochem J 478, 1959–1976.
Gillingham AK, Bertram J, Begum F, Munro S (2019). In vivo identification of GTPase interactors by mitochondrial relocalization and proximity biotinylation. Elife 8, e45916.
Gillingham AK, Sinka R, Torres IL, Lilley KS, Munro S (2014). Toward a comprehensive map of the effectors of rab GTPases. Dev Cell 31, 358–373.
Gillooly DJ, Raiborg C, Stenmark H (2003). Phosphatidylinositol 3-phosphate is found in microdomains of early endosomes. Histochem Cell Biol 120, 445–453.
Graham SC, Wartosch L, Gray SR, Scourfield EJ, Deane JE, Luzio JP, Owen DJ (2013). Structural basis of Vps33A recruitment to the human HOPS complex by Vps16. Proc Natl Acad Sci USA 110, 13345–13350.
Hämälistö S, Jäättelä M (2016). Lysosomes in cancer - living on the edge (of the cell). Curr Opin Cell Biol 39, 69–76.
Hämälistö S, Stahl JL, Favaro E, Yang Q, Liu B, Christoffersen L, Loos B, Guasch Boldú C, Joyce JA, Reinheckel T, *et al.* (2020). Spatially and temporally defined lysosomal leakage facilitates mitotic chromosome segregation. Nat Commun 11, 229.
Herrmann E, Langemeyer L, Auffarth K, Ungermann C, Kümmel D (2023). Targeting of the Mon1-Ccz1 Rab guanine nucleotide exchange factor to distinct organelles by a synergistic protein and lipid code. J Biol Chem 299, 102915.
Hille-Rehfeld A (1995). Mannose 6-phosphate receptors in sorting and transport of lysosomal enzymes. Biochim Biophys Acta 1241, 177–194.
Homewood CA, Warhurst DC, Peters W, Baggaley VC (1972). Lysosomes, pH and the anti-malarial action of chloroquine. Nature 235, 50–52.
Hu Y, Reggiori F (2022). Molecular regulation of autophagosome formation. Biochem Soc Trans 50, 55–69.
Huotari J, Helenius A (2011). Endosome maturation. EMBO J 30, 3481–3500.
Jiang P, Nishimura T, Sakamaki Y, Itakura E, Hatta T, Natsume T, Mizushima N (2014). The HOPS complex mediates autophagosome-lysosome fusion through interaction with syntaxin 17. Mol Biol Cell 25, 1327–1337.
Jongsma ML, Bakker J, Cabukusta B, Liv N, van Elsland D, Fermie J, Akkermans JL, Kuijl C, van der Zanden SY, Janssen L, et al. (2020). SKIP-HOPS recruits TBC1D15 for a Rab7-to-Arl8b identity switch to control late endosome transport. EMBO J 39, e102301.
Jonker CTH, Galmes R, Veenendaal T, Ten Brink C, van der Welle REN, Liv N, de Rooij J, Peden AA, van der Sluijs P, Margadant C, Klumperman J (2018). Vps3 and Vps8 control integrin trafficking from early to recycling endosomes and regulate integrin-dependent functions. Nat Commun 9, 792.
Kajiho H, Kajiho Y, Frittoli E, Confalonieri S, Bertalot G, Viale G, Di Fiore PP, Oldani A, Garre M, Beznoussenko GV, et al. (2016). RAB2A controls MT1-MMP endocytic and E-cadherin polarized Golgi trafficking to promote invasive breast cancer programs. EMBO Rep 17, 1061–1080.
Khatter D, Raina VB, Dwivedi D, Sindhwani A, Bahl S, Sharma M (2015). The small GTPase Arl8b regulates assembly of the mammalian HOPS complex on lysosomes. J Cell Sci 128, 1746–1761.
Kim BY, Krämer H, Yamamoto A, Kominami E, Kohsaka S, Akazawa C (2001). Molecular characterization of mammalian homologues of class C Vps proteins that interact with syntaxin-7. J Biol Chem 276, 29393–29402.
Klumperman J, Hille A, Veenendaal T, Oorschot V, Stoorvogel W, von Figura K, Geuze HJ (1993). Differences in the endosomal distributions of the two mannose 6-phosphate receptors. J Cell Biol 121, 997–1010.
Klumperman J, Raposo G (2014). The complex ultrastructure of the endolysosomal system. Cold Spring Harb Perspect Biol 6, a016857.
Kumar AV, Mills J, Lapierre LR (2022). Selective autophagy receptor p62/SQSTM1, a pivotal player in stress and aging. Front Cell Dev Biol 10, 793328.
Langemeyer L, Borchers A-C, Herrmann E, Füllbrunn N, Han Y, Perz A, Auffarth K, Kümmel D, Ungermann C (2020). A conserved and regulated mechanism drives endosomal Rab transition. eLife 9, e56090.
Laurent-Matha V, Derocq D, Prébois C, Katunuma N, Liaudet-Coopman E (2006). Processing of human cathepsin D is independent of its catalytic function and auto-activation: involvement of cathepsins L and B. J Biochem 139, 363–371.
Lie PPY, Nixon RA (2019). Lysosome trafficking and signaling in health and neurodegenerative diseases. Neurobiol Dis 122, 94–105.
Lin X, Yang T, Wang S, Wang Z, Yun Y, Sun L, Zhou Y, Xu X, Akazawa C, Hong W, Wang T (2014). RILP interacts with HOPS complex via VPS41 subunit to regulate endocytic trafficking. Sci Rep 4, 7282.
Liv N, Fermie J, Ten Brink CBM, de Heus C, Klumperman J (2023). Functional characterization of endo-lysosomal compartments by correlative live-cell and volume electron microscopy. Methods Cell Biol 177, 301–326.
Llinares E, Barry AO, André B (2015). The AP-3 adaptor complex mediates sorting of yeast and mammalian PQ-loop-family basic amino acid transporters to the vacuolar/lysosomal membrane. Sci Rep 5, 16665.
Lőrincz P, Juhász G (2020). Autophagosome-lysosome fusion. J Mol Biol 432, 2462–2482.
Lőrincz P, Tóth S, Benkő P, Lakatos Z, Boda A, Glatz G, Zobel M, Bisi S, Hegedűs K, Takáts S, et al. (2017). Rab2 promotes autophagic and endocytic lysosomal degradation. J Cell Biol 216, 1937–1947.
Lürick A, Kuhlee A, Bröcker C, Kümmel D, Raunser S, Ungermann C (2015). The Habc domain of the SNARE Vam3 interacts with the HOPS tethering complex to facilitate vacuole fusion. J Biol Chem 290, 5405.
Luzio JP, Parkinson MDJ, Gray SR, Bright NA (2009). The delivery of endocytosed cargo to lysosomes. Biochem Soc Trans 37, 1019–1021.
Mari M, Bujny MV, Zeuschner D, Geerts WJCC, Griffith J, Petersen CM, Cullen PJ, Klumperman J, Geuze HJ (2008). SNX1 defines an early endosomal recycling exit for sortilin and mannose 6-phosphate receptors. Traffic 9, 380–393.
Marques ARAA, Saftig P (2019). Lysosomal storage disorders - challenges, concepts and avenues for therapy: beyond rare diseases. J Cell Sci 132, jcs221739.
Mastronarde DN (2018). Advanced data acquisition from electron microscopes with SerialEM. Microsc Microanal 24, 864–865.
Mastronarde DN, Held SR (2017). Automated tilt series alignment and tomographic reconstruction in IMOD. J Struct Biol 197, 102–113.
Matsui T, Jiang P, Nakano S, Sakamaki Y, Yamamoto H, Mizushima N (2018). Autophagosomal YKT6 is required for fusion with lysosomes independently of syntaxin 17. J Cell Biol 217, 2633–2645.
McEwan DG, Popovic D, Gubas A, Terawaki S, Suzuki H, Stadel D, Coxon FP, MirandadeStegmann D, Bhogaraju S, Maddi K, *et al.* (2015). PLEKHM1 regulates autophagosome-lysosome fusion through HOPS complex and LC3/GABARAP proteins. Mol Cell 57, 39–54.
Mejlvang J, Olsvik H, Svenning S, Bruun J-A, Abudu YP, Larsen KB, Brech A, Hansen TE, Brenne H, Hansen T, *et al.* (2018). Starvation induces rapid degradation of selective autophagy receptors by endosomal microautophagy. J Cell Biol 217, 3640–3655.
Miao G, Zhao H, Li Y, Ji M, Chen Y, Shi Y, Bi Y, Wang P, Zhang H (2021). ORF3a of the COVID-19 virus SARS-CoV-2 blocks HOPS complex-mediated assembly of the SNARE complex required for autolysosome formation. Dev Cell 56, 427–442.e5.

Mizushima N (2020). The ATG conjugation systems in autophagy. Curr Opin Cell Biol 63, 1–10.
Monfrini E, Cogiamanian F, Salani S, Straniero L, Fagiolari G, Garbellini M, Carsana E, Borellini L, Biella F, Moggio M, *et al*. (2021a). A novel homozygous VPS11 variant may cause generalized dystonia. Ann Neurol 89, 834–839.
Monfrini E, Zech M, Steel D, Kurian MA, Winkelmann J, Di Fonzo A (2021b). HOPS-associated neurological disorders (HOPSANDs): linking endolysosomal dysfunction to the pathogenesis of dystonia. Brain 144, 2610–2615.
Mu FT, Callaghan JM, Steele-Mortimer O, Stenmark H, Parton RG, Campbell PL, McCluskey J, Yeo JP, Tock EPC, Toh BH (1995). EEA1, an early endosome-associated protein. EEA1 is a conserved α- helical peripheral membrane protein flanked by cysteine "fingers" and contains a calmodulin-binding IQ motif. J Biol Chem 270, 13503–13511.
Murray DH, Jahnel M, Lauer J, Avellaneda MJ, Brouilly N, Cezanne A, Morales-Navarrete H, Perini ED, Ferguson C, Lupas AN, *et al*. (2016). An endosomal tether undergoes an entropic collapse to bring vesicles together. Nature 537, 107–111.
Olson LJ, Misra SK, Ishihara M, Battaile KP, Grant OC, Sood A, Woods RJ, Kim JJP, Tiemeyer M, Ren G, *et al*. (2020). Allosteric regulation of lysosomal enzyme recognition by the cation-independent mannose 6-phosphate receptor. Commun Biol 3, 498.
Paul-Gilloteaux P, Heiligenstein X, Belle M, Domart MC, Larijani B, Collinson L, Raposo G, Salamero J (2017). EC-CLEM: Flexible multidimensional registration software for correlative microscopies. Nat Methods 14, 102–103.
Peng C, Ye J, Yan S, Kong S, Shen Y, Li C, Li Q, Zheng Y, Deng K, Xu T, Tao W (2012). Ablation of vacuole protein sorting 18 (Vps18) gene leads to neurodegeneration and impaired neuronal migration by disrupting multiple vesicle transport pathways to lysosomes. J Biol Chem 287, 32861–32873.
Peplowska K, Markgraf DF, Ostrowicz CW, Bange G, Ungermann C (2007). The CORVET tethering complex interacts with the yeast Rab5 homolog Vps21 and is involved in endo-lysosomal biogenesis. Dev Cell 12, 739–750.
Perini ED, Schaefer R, Stöter M, Kalaidzidis Y, Zerial M (2014). Mammalian CORVET is required for fusion and conversion of distinct early endosome subpopulations. Traffic 15, 1366–1389.
Pols MS, ten Brink C, Gosavi P, Oorschot V, Klumperman J (2013a). The HOPS proteins hVps41 and hVps39 are required for homotypic and heterotypic late endosome fusion. Traffic 14, 219–232.
Pols MS, van Meel E, Oorschot V, ten Brink C, Fukuda M, Swetha MG, Mayor S, Klumperman J (2013b). hVps41 and VAMP7 function in direct TGN to late endosome transport of lysosomal membrane proteins. Nat Commun 4, 1361.
Poteryaev D, Datta S, Ackema K, Zerial M, Spang A (2010). Identification of the switch in early-to-late endosome transition. Cell 141, 497–508.
Pu J, Guardia CM, Keren-Kaplan T, Bonifacino JS (2016). Mechanisms and functions of lysosome positioning. J Cell Sci 129, 4329–4339.
Raiborg C, Bache KG, Gillooly DJ, Madshus IH, Stang E, Stenmark H (2002). Hrs sorts ubiquitinated proteins into clathrin-coated microdomains of early endosomes. Nat Cell Biol 4, 394–398.
Reggiori F, Ungermann C (2017). Autophagosome maturation and fusion. J Mol Biol 429, 486–496.
Reitman ML, Varki A, Kornfeld S (1981). Fibroblasts from patients with I-cell disease and pseudo-Hurler polydystrophy are deficient in uridine 5′-diphosphate-N-acetylglucosamine: glycoprotein N-acetylglucosaminylphosphotransferase activity. J Clin Invest 67, 1574–1579.
Rieder SE, Emr SD (1997). A novel RING fringer protein complex essential for a late step in protein transport to the yeast vacuole. Mol Biol Cell 8, 2307–2327.
Rink J, Ghigo E, Kalaidzidis Y, Zerial M (2005). Rab conversion as a mechanism of progression from early to late endosomes. Cell 122, 735–749.
Saftig P, Klumperman J (2009). Lysosome biogenesis and lysosomal membrane proteins: Trafficking meets function. Nat Rev Mol Cell Biol 10, 623–635.
Sato TK, Rehling P, Peterson MR, Emr SD (2000). Class C Vps protein complex regulates vacuolar SNARE pairing and is required for vesicle docking/fusion. Mol Cell 6, 661–671.
Schindelin J, Arganda-Carreras I, Frise E, Kaynig V, Longair M, Pietzsch T, Preibisch S, Rueden C, Saalfeld S, Schmid B, *et al*. (2012). Fiji: An open-source platform for biological-image analysis. Nat Methods 9, 676–682.
Schleinitz A, Pöttgen L-A, Keren-Kaplan T, Pu J, Saftig P, Bonifacino JS, Haas A, Jeschke A (2023). Consecutive functions of small GTPases guide HOPS-mediated tethering of late endosomes and lysosomes. Cell Rep 42, 111969.
Schwartz ML, Nickerson DP, Lobingier BT, Plemel RL, Duan M, Angers CG, Zick M, Merz AJ (2017). Sec17 (α-SNAP) and an SM-tethering complex regulate the outcome of SNARE zippering in vitro and in vivo. eLife 6, e27396.
Seals DF, Eitzen G, Margolis N, Wickner WT, Price A (2000). A Ypt/Rab effector complex containing the Sec1 homolog Vps33p is required for homotypic vacuole fusion. Proc Natl Acad Sci 97, 9402–9407.
Seaman MNJ (2004). Cargo-selective endosomal sorting for retrieval to the Golgi requires retromer. J Cell Biol 165, 111–122.
Shvarev D, Schoppe J, König C, Perz A, Füllbrunn N, Kiontke S, Langemeyer L, Januliene D, Schnelle K, Kümmel D, *et al*. (2022). Structure of the HOPS tethering complex, a lysosomal membrane fusion machinery. eLife 11, e80901.
Simonetti B, Daly JL, Cullen PJ (2023). Out of the ESCPE room: Emerging roles of endosomal SNX-BARs in receptor transport and host-pathogen interaction. Traffic 24, 234–250.
Slot JW, Geuze HJ (2007). Cryosectioning and immunolabeling. Nat Protoc 2, 2480–2491.
Song H, Orr AS, Lee M, Harner ME, Wickner WT (2020). HOPS recognizes each SNARE, assembling ternary trans-complexes for rapid fusion upon engagement with the 4th SNARE. eLife 9, e53559.
Sriram V, Krishnan KS, Mayor S (2003). Deep-orange and carnation define distinct stages in late endosomal biogenesis in Drosophila melanogaster. J Cell Biol 161, 593–607.
Steel D, Zech M, Zhao C, Barwick KES, Burke D, Demailly D, Kumar KR, Zorzi G, Nardocci N, Kaiyrzhanov R, *et al*. (2020). Loss-of-function variants in HOPS complex genes VPS16 and VPS41 cause early onset dystonia associated with lysosomal abnormalities. Ann Neurol 88, 867–877.
Stenmark H (2009). Rab GTPases as coordinators of vesicle traffic. Nat Rev Mol Cell Biol 10, 513–525.
Stroupe C, Collins KM, Fratti RA, Wickner W (2006). Purification of active HOPS complex reveals its affinities for phosphoinositides and the SNARE Vam7p. EMBO J 25, 1579–1589.
Styers ML, Salazar G, Love R, Peden AA, Kowalczyk AP, Faundez V (2004). The endo-lysosomal sorting machinery interacts with the intermediate filament cytoskeleton. Mol Biol Cell 15, 5369–5382.
Swetha MG, Sriram V, Krishnan KS, Oorschot VMJ, ten Brink C, Klumperman J, Mayor S (2011). Lysosomal membrane protein composition, acidic pH and sterol content are regulated via a light-dependent pathway in metazoan cells. Traffic 12, 1037–1055.
Takáts S, Glatz G, Szenci G, Boda A, Horváth GV, Hegedűs K, Kovács AL, Juhász G (2018). Non-canonical role of the SNARE protein Ykt6 in autophagosome-lysosome fusion. PLoS Genet 14, e1007359.
Takáts S, Pircs K, Nagy P, Varga Á, Kárpáti M, Hegedűs K, Kramer H, Kovács AL, Sass M, Juhász G (2014). Interaction of the HOPS complex with Syntaxin 17 mediates autophagosome clearance in Drosophila. Mol Biol Cell 25, 1338–1354.
Terawaki S, Vasilev F, Moriwaki T, Otomo T (2023). HOPS, CORVET and newly-identified Hybrid tethering complexes contribute differentially towards multiple modes of endocytosis. Sci Rep 13, 18734.
van den Boomen DJH, Sienkiewicz A, Berlin I, Jongsma MLM, van Elsland DM, Luzio JP, Neefjes JJC, Lehner PJ (2020). A trimeric Rab7 GEF controls NPC1-dependent lysosomal cholesterol export. Nat Commun 11, 5559.
van der Beek J, de Heus C, Liv N, Klumperman J (2022). Quantitative correlative microscopy reveals the ultrastructural distribution of endogenous endosomal proteins. J Cell Biol 221, e202106044.
van der Beek J, Jonker C, van der Welle R, Liv N, Klumperman J (2019). CORVET, CHEVI and HOPS – multisubunit tethers of the endo-lysosomal system in health and disease. J Cell Sci 132, jcs189134.
van der Beek J, Veenendaal T, de Heus C, van Dijk S, Ten Brink C, Liv N, Klumperman J (Mar 31, 2023). Ultrastructural Localization of Endogenous LC3 by On-Section Correlative Light-Electron Microscopy. J Vis Exp, https://doi.org/10.3791/65067.
Van Der Kant R, Jonker CTH, Wijdeven RH, Bakker J, Janssen L, Klumperman J, Neefjes J (2015). Characterization of the mammalian CORVET and HOPS complexes and their modular restructuring for endosome specificity. J Biol Chem 290, 30280–30290.
van der Welle REN, Jobling R, Burns C, Sanza P, van der Beek JA, Fasano A, Chen L, Zwartkruis FJ, Zwakenberg S, Griffin EF, *et al*. (2021).

Neurodegenerative VPS41 variants inhibit HOPS function and mTORC1-dependent TFEB/TFE3 regulation. EMBO Mol Med 13, e13258.
van Meel E, Klumperman J (2014). TGN exit of the cation-independent mannose 6-phosphate receptor does not require acid hydrolase binding. Cell Logist 4, e954441.
van Weert AW, Dunn KW, Geuze HJ, Maxfield FR, Stoorvogel W (1995). Transport from late endosomes to lysosomes, but not sorting of integral membrane proteins in endosomes, depends on the vacuolar proton pump. J Cell Biol 130, 821–834.
Vietri M, Radulovic M, Stenmark H (2020). The many functions of ESCRTs. Nat Rev Mol Cell Biol 21, 25–42.
Waguri S, Dewitte F, Le Borgne RL, Rouillé Y, Uchiyama Y, Dubremetz J-F, Hoflack B (2003). Visualization of TGN to endosome trafficking through fluorescently labeled MPR and AP-1 in living cells. Mol Biol Cell 14, 142–155.
Wang CW, Stromhaug PE, Kauffman EJ, Weisman LS, Klionsky DJ (2003). Yeast homotypic vacuole fusion requires the Ccz1-Mon1 complex during the tethering/docking stage. J Cell Biol 163, 973–985.
Wang T, Yan L, Wang L, Sun J, Qu H, Ma Y, Song R, Tong X, Zhu J, Yuan Y, *et al*. (2023). VPS41-mediated incomplete autophagy aggravates cadmium-induced apoptosis in mouse hepatocytes. J Hazard Mater 459, 132243.
Wartosch L, Günesdogan U, Graham SC, Luzio JP (2015). Recruitment of VPS33A to HOPS by VPS16 is required for lysosome fusion with endosomes and autophagosomes. Traffic 16, 727–742.
Wegener CS, Malerød L, Pedersen NM, Prodiga C, Bakke O, Stenmark H, Brech A (2010). Ultrastructural characterization of giant endosomes induced by GTPase-deficient Rab5. Histochem Cell Biol 133, 41–55.
Wurmser AE, Sato TK, Emr SD (2000). New component of the vacuolar class C-Vps complex couples nucleotide exchange on the Ypt7 GTPase to SNARE-dependent docking and fusion. J Cell Biol 151, 551–562.
Yadati T, Houben T, Bitorina A, Shiri-Sverdlov R (2020). The ins and outs of cathepsins: physiological function and role in disease management. Cells 9, 1679.
Yang C, Wang X (2021). Lysosome biogenesis: regulation and functions. J Cell Biol 220, e202102001.
Yoshimori T, Yamamoto A, Moriyama Y, Futai M, Tashiro Y (1991). Bafilomycin A1, a specific inhibitor of vacuolar-type H+-ATPase, inhibits acidification and protein degradation in lysosomes of cultured cells. J Biol Chem 266, 17707–17712.
Yu L, Chen Y, Tooze SA (2018). Autophagy pathway: Cellular and molecular mechanisms. Autophagy 14, 207–215.
Zhang S, Tong M, Zheng D, Huang H, Li L, Ungermann C, Pan Y, Luo H, Lei M, Tang Z, *et al*. (2023). C9orf72-catalyzed GTP loading of Rab39A enables HOPS-mediated membrane tethering and fusion in mammalian autophagy. Nat Commun 14, 6360.
Zick M, Wickner W (2013). The tethering complex HOPS catalyzes assembly of the soluble SNARE Vam7 into fusogenic trans-SNARE complexes. Mol Biol Cell 24, 3746–3753.